Constitutive activation of cellular immunity underlies the evolution of resistance to infection in *Drosophila*

Alexandre B. Leitão[*1], Ramesh Arunkumar[*1], Jonathan P. Day[1], Emma M. Geldman[1], Ismaël Morin-Poulard[2], Michèle Crozatier[2], Francis M. Jiggins[1]

[1]Department of Genetics, University of Cambridge, Cambridge, United Kingdom

[2] Centre de Biologie du Développement, Centre de Biologie Intégrative, University Paul Sabatier, CNRS, 118 Route de Narbonne 31062 Toulouse cedex 09, France

* contributed equally

Abstract

Organisms rely on inducible and constitutive immune defences to combat infection. Constitutive immunity enables a rapid response to infection but may carry a cost for uninfected individuals, leading to the prediction that it will be favoured when infection rates are high. When we exposed populations of *Drosophila melanogaster* to intense parasitism by the parasitoid wasp *Leptopilina boulardi,* they evolved resistance by developing a more reactive cellular immune response. Using single-cell RNA sequencing, we found that immune-inducible genes had become constitutively upregulated. This was the result of resistant larvae differentiating precursors of specialized immune cells called lamellocytes that were previously only produced after infection. Therefore, populations evolved resistance by genetically hard-wiring the first steps of an induced immune response to become constitutive.

Introduction

A fundamental division within immune systems is between induced and constitutive immune defences. Constitutive immunity is always active, even in the absence of infection. For example, uninfected individuals produce natural antibodies(Savage et al., 2017), immune cells and antimicrobial peptides (AMPs) (Lemaitre and Hoffmann, 2007). In contrast, induced immune responses are triggered after infection, which frequently involve amplifying existing constitutive factors. This can include immune cells proliferating and differentiating, and the massive upregulation of AMPs and cytotoxic molecules (Lemaitre and Hoffmann, 2007). Constitutive immunity is fast, allowing hosts to avoid becoming infected altogether or to rapidly clear infections. However, immune defences can be costly, diverting limited resources from other fitness-related traits (Bajgar et al., 2015) or damaging the host through immunopathology (Graham et al., 2005; Sadd and Siva-Jothy, 2006). While induced immune responses only incur these costs after infection, they are always present for constitutive immunity, even in the absence of infection. This trade-off between speed and cost is predicted to govern the allocation of host investment into constitutive and induced immunity (Boots and Best, 2018; Shudo and Iwasa, 2001). Theoretical models predict that the key parameter determining which type of defence should be favoured is the frequency that hosts are exposed to infection—more frequent exposure favours constitutive defences (Shudo and Iwasa, 2001). In support of this, bacteria tend to evolve phage resistance by altering surface receptors when exposure is high and rely on induced CRISPR-Cas immunity when exposure is low (Westra et al., 2015). However, despite

there being variation in the extent of constitutive versus induced immunity within populations (Jent et al., 2019), to our knowledge the key prediction that high rates of parasitism lead to induced immune responses becoming constitutively expressed has not been demonstrated.

To investigate these questions, we examined how the constitutive and induced cellular immune defences of *Drosophila melanogaster* evolve under high parasite pressure. Cellular immunity in *D. melanogaster* involves blood cells called hemocytes, which play the equivalent role to leukocytes in vertebrates. In uninfected larvae there are two morphological and functional classes of hemocytes. Plasmatocytes constitute the majority of cells and have diverse functions including phagocytosis and AMP production (Honti et al., 2014). Crystal cells are a less abundant specialized cell type that produces the prophenoloxidase molecules PPO1 and PPO2, which are processed into enzymes required for the melanization of parasites and wound healing (Dudzic et al., 2015). Infection can trigger an induced response, where these cell types proliferate, and cells called lamellocytes differentiate from circulating plasmatocytes, and prohemocytes and plasmatocytes in the lymph gland (Cho et al., 2020; Honti et al., 2014). Lamellocytes are large flat cells with a specialised role in encapsulating and killing large parasites like parasitic wasps (parasitoids). When a parasitoid lays its egg into *D. melanogaster* larvae, plasmatocytes adhere to the egg. Then, as lamellocytes differentiate they create additional cellular layers known as a 'capsule'. Finally, the capsule is melanised by the activity of phenoloxidases produced in crystal cells and lamellocytes (Dudzic et al., 2015). The melanin physically encases the parasitoid and toxic by-

products of the melanisation reaction likely contribute to parasite killing (Nappi et al., 2009).

There is substantial genetic variation in susceptibility to parasitoid infection within *D. melanogaster* populations (Kraaijeveld and Godfray, 1999), and this is associated with an increase in the number of circulating hemocytes (Kraaijeveld et al., 2001; McGonigle et al., 2017). Here, we used a combination of experimental evolution with physiological assays and single-cell RNA sequencing to examine how a high rate of parasitism by the parasitoid wasp *L. boulardi* affects constitutive and induced immune defences.

Results

The evolution of resistance is associated with a more reactive immune response

To investigate the evolution of the cellular immune response, we allowed genetically diverse populations of *D. melanogaster* to evolve under intense levels of parasitism. We established an outbred population from 377 wild-caught *D. melanogaster* females, and used this to found six experimental populations that were maintained at population sizes of 200 flies. In three of these populations, larvae were infected every generation, and flies that survived by encapsulating and melanising the wasp were used to establish the next generation (Figure 1A, High Parasitism populations). The other three populations were maintained in the same conditions but without infection (Figure 1A, No Parasitism populations). In line with previous studies (Fellowes et al., 1998; McGonigle et al., 2017), the High Parasitism populations increased in resistance over the

92 generations (Figure 1B, Selection regime x Generation: χ^2= 91.41, d.f.= 1, p<10^{-15}). After 33 generations, a mean of 76% of flies survived infection in the High Parasitism populations, compared to 10% in the No Parasitism controls.

95

96 As populations evolved resistance, they melanised parasitoids at a higher rate
97 (Figure 1B). This could result from increased activity of the encapsulation
98 immune response, or because the flies are evolving to escape the effects of
99 immunosuppressive molecules produced by the parasite. To distinguish these
100 possibilities, we measured the ability of each population to react to an inert
101 object. When a small volume of paraffin oil is injected into the larval haemocoel,
102 it remains as a sphere and can be encapsulated (Havard et al., 2009). Populations
103 that evolved without parasitism show a very limited reaction to the oil droplets
104 (Figure 1C). In contrast, approximately half of larvae from selected populations
105 encapsulate the oil droplet (Figure 1C; Selection Regime: χ^2= 73.35, d.f= 1,
106 p=2x10^{-16}). Therefore, high levels of parasitism led to the cellular immune
107 system evolving a more active encapsulation response.

108

109 **Constitutive upregulation of immune-induced genes**

110 Underlying induced immune responses is a transcriptional response to infection,
111 so we examined how the hemocyte transcriptome altered in populations that
112 evolved under high levels of parasitism. We harvested circulating hemocytes
113 from *Drosophila* larvae and sequenced the transcriptomes of individual cells
114 using the 10X Genomics platform. Initially, we pooled and jointly analysed
115 RNAseq reads sequenced from all cells, effectively treating them as 'bulk'
116 RNAseq data. This allowed us to investigate global changes in hemocyte gene

117 expression following infection and adaptation to high rates of parasitism (Figure
118 2A).

119

120 Forty-eight hours after flies were infected with parasitoid wasps there was a
121 strong transcriptional response to infection (Figure 2B-C). Strikingly, when flies
122 adapted to high parasitism conditions they showed similar transcriptional
123 changes, even when uninfected. This can be seen by comparing the induced
124 changes in gene expression that occur after infection to the constitutive changes
125 in gene expression that occur after adapting to high rates of parasitism (Figure
126 2B, 2: Y axis). Taking the 173 genes that had at least a 50% change in transcript
127 levels after infection or selection, in every case the direction of change was the
128 same after infection and adaptation to high parasitism (Figure 2B). These genes
129 were enriched for biological roles such as cytoskeletal organization and cell
130 adhesion (Supplementary file 1). We verified that the evolved response
131 mimicked the induced response by using quantitative PCR (qPCR) to measure
132 the expression of the lamellocyte marker *atilla* and the anti-parasitoid effector
133 gene *PPO3* (Figure 2 — figure supplement 1). Again, we found that high rates of
134 parasitism led to these immune-induced genes becoming constitutively
135 upregulated. Therefore, as populations evolved resistance, the induced
136 transcriptional response to infection has become in part genetically hard-wired
137 and constitutive.

138

139 We took the same approach to examine how the induced transcriptional
140 response to infection changed as populations evolved resistance. We found that

the transcriptional response to infection involved the same genes in the different populations (Figure 2B versus 2C). However, the magnitude of the changes in gene expression was substantially less in populations that had evolved under high parasite pressure (Figure 2B versus 2C). Therefore, the increase in constitutive gene expression has been matched by a decrease in induced expression. Again, this was verified by qPCR (Figure 2 — figure supplement 1). This is consistent with there being a 'maximum' level of expression of these genes, so an increase in constitutive gene expression will lead to a decrease in induced expression. In support of this, combining the constitutive and induced changes in gene expression, the hemocyte transcriptome after infection is similar in the populations that evolved under high levels of parasitism and the controls (Figure 2C). Therefore, an induced response has become genetically fixed, as opposed to selection leading to a greater total response.

scRNA-seq reveals novel hemocyte types

The global changes in hemocyte transcriptomes could result from a change in the relative proportion of cell types in the hemocyte population, or from a shift in gene expression within existing cell types. We therefore used the same data analysed above but investigated gene expression within individual cells. The three classical *Drosophila* hemocyte types were originally defined morphologically, but emerging single cell transcriptomic data suggests that *Drosophila* hemocyte populations are more complex than this (Cattenoz et al., 2020; Cho et al., 2020; Fu et al., 2020; Gopal Tattikota et al., 2019). Excluding cells that did not express the pan-hemocyte markers *Hemese* or *Serpent*

(Banerjee et al., 2019; Vivancos and Giangrande, 1997), we grouped 19,344 larval hemocytes into nine clusters based on their transcriptomes (Figure 3A). Neither infection nor selection leads to the appearance of new cell states (Figure 3B).

We identified two large clusters of plasmatocytes. The largest was PLASM1, which we classify as the cycling plasmatocyte state as it had the greatest number of replicating cells in the G2M or S phase (Figure 3—figure supplement 1). The 5,712 cells in this cluster had high expression of genes associated with plasmatocytes (*Col4a1*, *Pxn*, *eater*, *Hml*, *NimC1* (Banerjee et al., 2019)) and actively replicating cells (*stg* (Edgar and O'Farrell, 1990), *polo* (Glover, 2005)and *scra* (Oegema et al., 2000)) (Figure 3—figure supplement 2A). The next largest cluster, PLASM2, contained 2,874 plasmatocytes that were enriched for the genes encoding rRNA (Figure 3—figure supplement 2B) or involved in the ribosome biogenesis (Supplementary file 2). There were two smaller plasmatocyte clusters. The AMP cluster contained 196 cells with elevated expression of genes encoding antimicrobial and antifungal peptides, including *Drs*, *Mtk* and *CecA1* (Lemaitre and Hoffmann 2007, Figure 3—figure supplement 2B; Supplementary file 2). The MET cluster contained 283 cells with high expression of the heat shock proteins *Hsp24* and *Hsp27* and genes involved in organic acid metabolism (Figure 3—figure supplement 2B; Supplementary file 2). The crystal cells formed a single cluster of 906 cells (Figure 3A). Three clusters of cells, LAM 1, 2 and 3, had elevated expression of one or more lamellocyte marker genes (Banerjee et al., 2019) (Figure 3—figure supplement 2C) and contained 1,260, 5,104 and 3,000 cells respectively.

Two similar scRNA-seq studies of *D. melanogaster* larval hemocytes have recently been published, so we investigated whether they identified similar clusters of cells to us (Cattenoz et al., 2020; Gopal Tattikota et al., 2020). For each of the three datasets, we assigned cells to the clusters identified in the other two studies. We found that all three analyses identified very similar clusters of crystal cells, lamellocytes and AMP-expressing plasmatocytes (Figure 3—figure supplement 3). However, there was less correspondence between studies for the other clusters of plasmatocytes (Figure 3—figure supplement 3).

Inducible cell states are present constitutively in resistant populations

Lamellocytes are key effector cells in the anti-parasitoid immune response. In populations that evolved without exposure to parasitoids, infection resulted in a large increase in the number of cells in all three lamellocyte clusters (LAM1-3, Figure 3B-C). In populations that evolved under high levels of parasitism, this inducible response become constitutive, with uninfected larvae having 3-5 fold more cells in LAM1 and 2 (Figure 3C). However, this was matched by a reduction in the induced response, so the final number of cells in these clusters after infection was similar regardless of whether the populations had adapted to high or low parasitism rates (Figure 3B-C). These results held when replicate populations were analyzed separately (Figure 3—figure supplement 5A, B) or when the number of cells in each library were down-sampled to match the library with the least number of cells (Figure 3—figure supplement 5C).

Therefore, when populations evolved under high infection rates this led to the differentiation of specialised immune cells occurring in uninfected individuals.

To investigate the developmental origins of this change, we reconstructed the pathway by which plasmatocytes differentiate into mature lamellocytes. By subclustering the cells and ordering them along a pseudotemporal scale, we found a single lineage starting from the self-cycling plasmatocytes (PLASM1) and ending in LAM3 (Fig. 4A). Along this lineage there was a decrease in cell replication, with the largest fraction of cells in the G2M and S phase in PLASM1 and the largest fraction in G1 in LAM3 (Figure 4—figure supplement 1A). Importantly, controlling for the effects of cell cycle had a negligible impact on the clustering (Supplementary file 4) and the trajectory of lamellocyte differentiation (Figure 4—figure supplement 1B). The expression of numerous genes changed as cells progressed along this trajectory (Figure 4—figure supplement 1C, Supplementary file 5), including increases in the expression of the lamellocyte effector gene *PPO3* and the lamellocyte marker *atilla* (Figure 4B, 4C). To understand the functional significance of the changes we used a gene ontology analysis. Genes involved in actin-filament based processes and biological adhesion were significantly upregulated in the terminal lamellocyte cluster, possibly reflecting the changes in cell morphology and the role of lamellocytes in capsule formation (Figure 4D). On the other hand, genes involved in extracellular structure organization were down-regulated as cells differentiated (Figure 4D and Supplementary file 6). This likely reflects the loss of the ability of cells to secrete extracellular matrix, which is a house-keeping function of plasmatocytes (Bunt et al., 2010; Olofsson and Page, 2005). Together, these results suggest that LAM1 and LAM2 cells are immature lamellocytes,

while LAM3 cells are mature lamellocytes. Consistent with this finding, the mature lamellocyte cluster LAM3 strongly corresponds to mature lamellocyte clusters defined in previously published larval hemocyte scRNA-seq data sets (Cattenoz et al., 2020 - LM-1; Tattikota et al., 2020 - LM2) (Figure 3—figure supplement 3). Similarly, the immature lamellocyte clusters, LAM1 and 2, match the immature lamellocyte clusters in those studies (Cattenoz et al., 2020 - LM-2; Tattikota et al., 2020 - LM1) (Figure 3—figure supplement 3).

Comparing our populations, the inducible production of immature lamellocytes (LAM1 and 2) has become entirely constitutive in the populations evolved under high rates of parasitism, while the production of mature lamellocytes (LAM3) response remains largely inducible (Figure 3C). The differentiation of these cells explains the changes in gene expression that we observed in pooled cells after infection or selection (Fig. 1)—168 of the 173 genes with at least a 50% change in expression in Figure 1 also change expression in the same direction as cells differentiate from plasmatocytes into lamellocytes (PLASM1 vs LAM3). Together these results suggests that high infection rates result in the cellular immune response becoming 'primed' by constitutively producing the precursors of the cells required for parasite killing.

Morphological differentiation of lamellocytes remains an inducible response

Lamellocytes are classically defined morphologically as large flattened cells. As expected, the proportion of morphologically identifiable lamellocytes increased after infection (Figure 5A and Figure 5 — figure supplement 1; Treatment: χ^2=

48.14, d.f= 1, p=3.97x10^{-12}). However, in contrast to our analysis of single cell transcriptomes, there was little difference between selection regimes in the proportion of these cells in either infected or uninfected larvae (Figure 5A and Figure 5 — figure supplement 1; Selection regime x Treatment: χ^2= 0.16, d.f= 1, p=0.69; Selection regime: χ^2= 0.41, d.f= 1, p=0.52). This suggests that while the transcriptional state of cells has been constitutively activated, the change in cell morphology, corresponding to the final step of lamellocytes maturation, remains an inducible response. These cells may be equivalent to hemocytes called lamelloblasts, which morphologically resemble plasmatocytes but are induced by parasitoid infection and likely give rise to lamellocytes (Anderl et al., 2016). To test this hypothesis, we used microscopy to measure both cell morphology and, as a marker of the transcriptional state of the cells, atilla expression (Figure 5 — figure supplement 2). In line with our scRNAseq data, both infection and adaptation to high parasitism rates increases the proportion of atilla positive cells (Figure 5C; Selection Regime x Treatment: F=25.7, d.f=1,8, p=0.0009). However, among the atilla positive cells, infection had a large effect on cell size (Fig. 5C; Treatment: F=41.6, d.f.=1,7, p=0.0003), while selection had a small effect (Fig. 5C; Selection Regime: F=4.9, d.f.=1,7, p=0.06). Therefore, while selection has resulted in the constitutive transcriptional activation of cells, changes in lamellocyte morphology remain largely an inducible response.

High parasitism rates lead to changes to hematopoiesis

In addition to the change in the transcriptional state of cells in circulation, we found that the populations maintained under strong parasite pressure evolved a constitutive increase in the number of hemocytes in circulation (Figure 5B and

Figure 5 — figure supplement 1; Selection regime: χ^2= 22.37, d.f= 1, p=2.25x10^{-6}). This increase in circulating hemocytes supports results from previous selection experiments (Kraaijeveld et al., 2001; McGonigle et al., 2017) and comparative analyses (Eslin and Prevost, 1998). *Drosophila* populations can increase the number of circulating hemocytes by relocating sessile hemocytes into circulation or by increasing the total number of hemocytes (McGonigle et al., 2017). We found that populations maintained under the high parasitism regime increased the total number of hemocytes, rather than move cells from the sessile compartment into circulation (Figure 5 — figure supplement 5; Selection regime: χ^2= 34.79, d.f= 1, p=3.67x10^{-9}; Selection regime * Compartment: χ^2= 2.41, d.f= 1, p=0.12). In accordance with this result, the number of crystal cells in the sessile compartment was not altered in populations maintained with high parasitism (Figure 5 — figure supplement 6; Selection regime: χ^2= 0.014, d.f= 1, p=0.91). The increase in hemocyte number is another aspect of the induced response that has become constitutive.

Lamellocytes can differentiate from sessile or circulating plasmatocytes, or from cells in the lymph gland, which is the larval hematopoietic organ. To investigate how adaptation to high parasitism conditions affected this organ, we performed immunostainings with antibodies recognizing two integrin subunits, *myospheroid* (*mys*) and the *Integrin alphaPS4 subunit* (α-*PS4*) (Figure 5 — figure supplement 3). Immature lamellocytes are *mys*$^{+}$ *a-PS4*$^{-}$ whereas mature lamellocytes are *mys*$^{+}$ *a-PS4*$^{+}$ (Louradour et al., 2017). Mature and immature lamellocytes are detected in larvae raised with and without parasitism both in mid and late L3 stage (Figure 5D and Figure 5 – figure supplement 3). However,

310 populations that adapted to high rates of parasitism have a higher number of
311 lymph glands containing immature lamellocytes (Figure 5D; main effect selection
312 regime: χ^2= 6.90, d.f.= 1, p=0.009), and a non-significant trend towards a higher
313 number of mature lamellocytes (Figure 5D ; main effect selection regime: χ^2=
314 3.13, d.f.= 1, p=0.08). We also analysed lymph gland disruption. In the absence of
315 parasitism, lymph glands remain intact until metamorphosis (Grigorian et al.,
316 2011). In response to parasitism by wasps, the larval organ is prematurely
317 disrupted, leading to the release of lymph gland hemocytes in circulation
318 (Louradour et al., 2017). Across all our populations, in the absence of wasp
319 parasitism, we found that at least 25% of lymph glands were disrupted (Figure
320 5E and figure 5 – supplement 3). Furthermore, in populations raised under high
321 parasitism the proportion of disrupted lymph glands increased up to 60% at the
322 late L3 larval stage (Figure 5E; selection regime*larval stage: χ^2=3.46, d.f.=1,
323 p=0.06). Therefore, adaptation to high parasitism leads to an increase in both the
324 differentiation of lamellocyte precursors in the lymph gland and the premature
325 disruption of lymph glands. Together our analyses of both circulating hemocytes
326 and lymph glands indicate that the *Drosophila* populations that evolved under
327 the high parasitism regime are primed for lamellocyte differentiation.
328
329 Based on our analyses of both circulating hemocytes and lymph glands, we
330 hypothesised that accelerated lamellocyte production during infection underlies
331 the evolution of resistance. To investigate this hypothesis, we counted the
332 number of hemocytes during the course of infection (Figure 5 — figure
333 supplement 4). In line with our earlier results, infected larvae from populations
334 selected under high parasitism produced more hemocytes overall and more

lamellocytes specifically (total hemocytes, selection regime: χ^2= 70, d.f.= 1, p<2.2x10^{-16}; lamellocytes, selection regime: χ^2= 14.92, d.f.= 1, p=0.11x10^{-3}). Supporting our hypothesis, the dynamics of lamellocyte production differs between selection regimes, with populations selected under high parasitism producing higher proportions of lamellocytes at earlier time points (Figure 5 — figure supplement 4; Lamellocyte proportion, selection regime*time point: χ^2= 36.56, d.f.= 3, p=5.69x10^{-8}). At the early timepoint of 12 hours post infection, lamellocyte concentration was eight times higher in the populations that had evolved under high parasitism rates while total hemocytes was 2.5 times higher (Figure 5 — figure supplement 4). This fast increase in circulating hemocytes numbers is likely explained by a combination of cell proliferation and relocation of sessile hemocytes into circulation, since lymph glands take longer to respond to parasitism (Sorrentino et al., 2002). Altogether, these results support the hypothesis that constitutive activation of immune defences allows hosts to mount more rapid immune responses.

Discussion

Our results support the hypothesis that natural selection favours constitutive defences when infection is common (Boots and Best, 2018; Shudo and Iwasa, 2001; Westra et al., 2015) by demonstrating that an inducible immune response becomes constitutive when populations frequently encounter a parasite. The induced immune response to parasitoids relies on the differentiation of lamellocytes from embryonic-derived plasmatocytes, lymph gland prohemocytes (Honti et al., 2014) and lymph gland plasmatocytes (Cho, 2020). Evidence for immature lamellocytes during infection has previously come from patterns of

marker gene expression (Anderl et al., 2016; Honti et al., 2010) and recent scRNAseq data (Cattenoz et al., 2020; Gopal Tattikota et al., 2019). Our results show that *Drosophila* populations evolve to produce these cells constitutively if they are frequently exposed to infection. Our results contrast with populations evolved with high levels of parasitism by the parasitoid wasp *Asobara tabida*, where there was no significant overlap of differentially expressed genes between selection and infection (Wertheim et al., 2011). These results were generated by sequencing RNA extracted from the whole larval body (Wertheim et al., 2011), so it is likely they may have missed changes in gene expression that occur in only a subset of immune cells. The difference between the studies could also result from the different genetic basis of resistance to the two wasp species (Poirie et al., 2000).

The change in the transcriptional state of constitutive cells was not accompanied by morphological differentiation, suggesting that populations that adapt to high parasitism rates have their cellular immune defences in a state of readiness, with the final step of massive lamellocyte differentiation remaining an inducible response. Genes involved in cytoskeleton dynamics such as *βTub60D* and *shot* are among the genes with the greatest increases in expression as lamellocytes differentiate (Figure 4—figure supplement 1C, Supplementary file 5) and these may be required for the final step of changing cell shape (Rizki and Rizki, 1994). Furthermore, the late stages of the immune response were not qualitatively altered after selection. Populations from both selection regimes had very similar hemocyte compositions in the late stages of the response, which is similar to

patterns reported from populations artificially selected with *Asobara tabida* (Salazar-Jaramillo et al., 2017).

Evolving resistance to parasitoid wasps is costly in *Drosophila* (Fellowes et al., 1998; Kraaijeveld and Godfray, 1997; McGonigle et al., 2017), so inducible immunity may be an adaptation that allows uninfected individuals to avoid this cost under low parasitism conditions. The physiological mechanism that causes the cost is unknown. It is possible that the differentiation of immature lamellocytes diverts resources from other fitness related traits as lamellocyte differentiation is energy-demanding (Bajgar et al., 2015). Trehalose is the most abundant circulating sugar in insects, and it can be cleaved into glucose by the enzyme trehalase (Mattila and Hietakangas, 2017). In support of previous results, we found that *Trehalase* and the trehalose transporter *Tret1-1* are upregulated in hemocytes after parasitoid infection (Figure 2; Bajgar et al., 2015). Together with increased expression of glycolysis genes after infection, this is thought to redirect energy from development to immunity (Bajgar et al., 2015). We found that these genes are also upregulated in uninfected larvae after adaptation to high parasitism pressure (Figure 2). This suggests that the metabolic cost of immunity may be borne by uninfected flies in our resistant populations, potentially contributing to the cost of evolving resistance.

After infection, whether the host or parasitoid survives is a race between parasitoid development and the formation of a cellular capsule by the immune system (Kim-Jo et al., 2019). To increase their success, parasitoid wasps inject venom proteins and virus like particles (VLPs) during oviposition to supress the

409 host immune system (Labrosse et al., 2003). These factors affect different
410 components of the immune system (Poirié et al., 2014), with the *L. boulardi*
411 strain used in this study affecting lamellocyte differentiation (Leitão et al., 2019).
412 Thus, resistant populations must circumvent the suppressive effects of the wasp
413 venoms and VLPs, and constitutive activation of cellular immunity may be a way
414 to achieve this by killing the parasite before immunity is suppressed.
415
416 We find that populations adapted to high levels of parasitism evolved two
417 phenotypes that likely explain their higher resistance. Firstly, they produce more
418 hemocytes in homeostasis, which leads to a faster increase in circulating
419 hemocytes in early time points of infection. Secondly, they produce lamellocytes
420 more rapidly upon infection, likely largely due to the constitutive production of
421 immature lamellocytes. Furthermore, cytotoxic molecules could be more readily
422 available as there is an increase in the constitutive expression of *PPO3* in
423 populations adapted to high rates of parasitism. *PPO3* encodes a intracellular
424 prophenoloxidase produced by lamellocytes that, when activated, is responsible
425 for the capsule melanization (Dudzic et al., 2015). We conclude that the
426 constitutive activation of the cellular immune response likely explains the
427 greatly increased resistance of populations adapted to high rates of parasitism.
428
429 **Methods**

430 **Key Resources Table**

Reagent type (species) or resource	Designation	Source or reference	Identifiers	Additional information
software, algorithm	GitHub	https://github.com/	RRID:SCR_002630	
software, algorithm	LSD	cran		https://cran.r-project.org/web/packages/LSD/index.html
software, algorithm	MAST	doi: 10.1186/s13059-015-0844-5.		
software, algorithm	tidymodels	cran		https://www.tidymodels.org/
software, algorithm	ranger	cran		https://cran.r-project.org/web/packages/ranger/index.html
software, algorithm	R	http://www.r-project.org/	RRID:SCR_001905	
software, algorithm	EBI database	doi: 10.1093/nar/gkz268.	RRID:SCR_004727	
software, algorithm	Sequence Read Archive	http://www.ncbi.nlm.nih.gov/sra	RRID:SCR_004891	
software, algorithm	pheatmap	https://www.rdocumentation.org/packages/pheatmap/versions/0.2/topics/pheatmap	RRID:SCR_016418	
software, algorithm	ArrayExpress	http://www.ebi.ac.uk/arrayexpress/	RRID:SCR_002964	
software, algorithm	Gene Expression Omnibus	https://www.ncbi.nlm.nih.gov/geo/	RRID:SCR_005012	
software, algorithm	REViGO	doi: 10.1371/journal.pone.0021800.	RRID:SCR_005825	
software, algorithm	gridExtra	cran		https://cran.r-project.org/web/packages/gridExtra/index.html
software, algorithm	cowplot	cran	RRID:SCR_018081	https://cran.r-project.org/web/packages/cowplot/index.html
software, algorithm	tidyverse	cran	RRID:SCR_019186	https://CRAN.R-project.org/package=tidyverse
software, algorithm	limma	doi: 10.1093/nar/gkv007.	RRID:SCR_010943	
software, algorithm	Slingshot	doi: 10.1186/s12864-018-4772-0.	RRID:SCR_017012	
software, algorithm	KEGG	doi: 10.1093/nar/gkj102.	RRID:SCR_012773	
software, algorithm	Reactome	doi: 10.1093/nar/gkv1351.	RRID:SCR_003485	
software, algorithm	Cell Ranger	https://support.10xgenomics.com/single-cell-gene-expression/software/overview/welcome	RRID:SCR_017344	
software, algorithm	Seurat	doi:10.1016/j.cell.2019.05.031	RRID:SCR_007322	
software, algorithm	Flymine	doi:10.1186/gb-2007-8-7-r129	RRID:SCR_002694	
strain, strain background (*Drosophila melanogaster*)	CAMOP3	This paper	CAMOP3	Outbred population of *D.melanogaster*
antibody	anti-Atilla (mouse monoclonal)	doi: 10.1556/ABiol.58.2007.Suppl.8	L1	1 in 100
antibody	anti-alphaPS4 (rabbit polyclonal)	doi: 10.1038/nature05650		1 in 200
antibody	anti-Mys (mouse monoclonal)	Developmental Studies Hybridoma Bank	RRID: AB_528310C; Cat#:F.6G11c	1 in 100

sequence-based reagent	PPO3_qPCR_2_Fw	This paper	qPCR primers	GATGTGGACCGGCCTAACAA
sequence-based reagent	PPO3_qPCR_2_Rev	This paper	qPCR primers	GATGCCCTTAGCGTCATCCA
sequence-based reagent	atilla_qPCR2_Fw	This paper	qPCR primers	ACCCACCAAATATGCTGAAACA
sequence-based reagent	atilla_qPCR2_Rv	This paper	qPCR primers	TTGATGGCCGATGCACTGT
sequence-based reagent	RpL32_qPCR_F-d	https://doi.org/10.1371/journal.ppat.1004728	qPCR primers	TGCTAAGCTGTCGCACAAATGG
sequence-based reagent	RpL_qPCR_R-h	https://doi.org/10.1371/journal.ppat.1004728	qPCR primers	TGCGCTTGTTCGATCCGTAAC
Other	Phalloidin staining	Invitrogen	RRID: AB_2315633; Cat. #: A12381	1 in 2000
Other	Mineral oil	Sigma-Aldrich	Cat#: M5904	

Artificial selection

An outcrossed *D. melanogaster* population was founded from the progeny of 377 females collected in July 2018 from banana and yeast traps set up in an allotment plot in Cambridge, UK (52°12'12.5"N 0°09'00.6"E). Single females were sorted into vials with cornmeal food (per 1200ml water: 13g agar, 105g dextrose, 105g maize, 23g yeast, 35ml Nipagin 10% w/v) to create isofemale lines. From the progeny of each isofemale line, 5 females and 5 males lines were sorted into a population cage to create the source population with 3770 flies. Flies from the source population were allowed to lay eggs overnight in 90mm agar plates (per 1500ml water: 45g agar, 50g dextrose, 500ml apple juice, 30ml Nipagin 10% w/v) spread with yeast paste (*Saccharomyces cerevisiae* – Sigma-Aldrich #YSC2). Eggs were removed from the agar plate with phosphate buffered saline (PBS) and a paintbrush, collected in 15ml centrifuge tubes and allowed to settle on the bottom of the tube. 500µl of egg solution were transferred into a 1.5ml microcentrifuge tube. 5µl of egg solution were transferred into plastic vials with cornmeal food and incubated at 25°C, in a 14 hours light/10 hours dark cycle and 70% humidity. 48 hours after egg transfer, a single female wasp was added into vials for infection treatments and allowed to infect larvae for 24 hours. Vials from infection and no infection treatments were incubated for 12 days in total. Flies from infection treatment with visible capsules were collected and randomly sorted into triplicate selection lines (NSRef1-3). Flies from no infection treatment were sorted into triplicate control populations (C1-3). Consecutive generations of selection were maintained with the same protocol described.

455 Population sizes were maintained at 200 adult flies for all populations, at
456 roughly 50% sex ratio.

457

458 **Estimation of encapsulation ratio**

459 To determine encapsulation ability, 10 vials per line were prepared without
460 infection and 20 vials with infection according to the selection protocol
461 described above. Flies emerging from the no infection vials (control flies) were
462 counted. Flies from infected vials were discriminated for the presence/absence
463 of capsules by squishing anesthetized flies between two glass slides and
464 observing under a dissecting microscope. Encapsulation ratio was calculated
465 according to the formula:

$$Encapsulation\ Ratio = \frac{Capsules}{Control - Uninfected}$$

466 In the formula, Capsules represent the mean number of flies from infection vials
467 with visible capsules and Uninfected represent the mean number of flies with no
468 discernable capsule. Control represent the mean number of flies from vials with
469 no infection. With this method we have an estimate of proportion of infected flies
470 with successful encapsulation per line.

471

472 **Wasp maintenance**

473 *Leptopilina boulardi* strain NSRef (Varaldi et al., 2006) was maintained in a very
474 susceptible *D. melanogaster* outbreed population named CAMOP2. Cornmeal
475 vials were prepared with 6µl of eggs as described above. Two female wasps and
476 one male were added to each vial. Vials were incubated for 24 days at 25°C, in a

14 hours light/10 hours dark cycle and 70% humidity. Adult wasps were collected and maintained in cornmeal vials with a drop of honey.

Oil injection

Egg solutions were prepared in 1.5ml microcentrifuge tubes as described above. 15µl of eggs were transferred into 50mm diameter plastic plates with cornmeal food. Plates were incubated for 72h at 25°C. Borosilicate glass 3.5" capillaries (Drummond Scientific Co. 3-000-203-G/X) were pulled to form thin needles in a needle puller (Narishige PC-10). The needle was backfilled with paraffin oil (Sigma-Aldrich #M5904) with a syringe and attached to a nanoinjector (Drummond Scientific Co. Nonoject II). Late 2nd instar and early 3rd instar larvae were carefully removed with forceps from cornmeal food plates and placed on filter paper, in groups of 20. Larvae were carefully injected with 4.6nl of oil. After injection, $_{dd}H_20$ was added with a brush to remove the larvae and a total of 40 larvae were transferred into a cornmeal food vial and incubated at 25°C. After 48 hours larvae were removed with a 15% w/v sugar solution and transferred into $_{dd}H_2O$ droplets on top of a plastic plate. Larvae were observed under a dissecting microscope and scored for the presence of melanization in the oil droplet.

Hemocyte counts

To estimate hemocyte concentration, eggs were transferred into cornmeal vials following the artificial selection protocol described above and incubated at 25°C. In infection treatment vials, 3 female wasps were allowed to infect larvae for 3 hours, 48 hours post egg transfer. This protocol guarantees a high infection ratio

(Leitão et al., 2019) and reduces the time window for the treatment. To count hemocytes during the course of experimental evolution, vials were incubated 48h post infection. To estimate hemocyte numbers during the course of infection, vials were incubated for 12, 24, 36 and 48h post infection. 3rd instar larvae were collected from the food vials, washed in $_{dd}H_2O$, dried in filter paper and transferred to a multispot porcelain plate in groups of 10. Hemolymph was collected by tearing the larval cuticle from the ventral side. 2µl of hemolymph were rapidly collected and diluted in 8µl of Neutral Red (1.65g/L PBS – Sigma-Aldrich #N2889) to help visualize the cells. The diluted hemolymph was transferred into a Thoma chamber and the number of hemocytes in 0.1µl was counted. Plasmatocytes and lamellocytes were distinguished by morphology (Rizki, 1957). To relocate hemocytes from sessile compartments into circulation, groups of 10 larvae were transferred into a 2ml microcentrifuge tube with 0.5ml water and 0.5g of glass beads (425-600µm, Sigma #G9268). The tubes were then vortexed at maximum speed for 1min (Petraki et al., 2015) and larvae prepared for hemolymph collection as described above.

Crystal cell counts

Third instar larvae were collected as described above, transferred to a microcentrifuge tube with 1ml PBS and heated at 68°C for 15 min. This treatment induces the spontaneous activation of PPO in hemocytes, allowing the identification of sessile crystal cells (Dudzic et al., 2015). The posterior dorsal part of individual larvae was imaged and crystal cells on the A7 segment manually counted.

Quantitative PCR

To analyze the expression of *PPO3* and *atilla*, RNA was extracted from hemocytes pooled from 50-70 larvae, 24h post infection. Larvae were cleaned in $_{dd}H_2O$, dried in filter paper and transferred into a well of a multispot porcelain plate with 100µl of PBS. Hemolymph was collected by tearing the ventral side of the larval cuticle. Samples were homogenized in 400µl TRIzol [Ambion #15596018] and kept at -80°C. For RNA extraction, samples were defrosted and centrifuged for 10min at 4°C at 12.000g. 160µl of supernatant was transferred into 1.5ml microcentrifuge tubes, 62.5µl of chloroform [Fisher Scientific #C/4920/08] was added, tubes were shaken for 15s and incubated for 3min. After a 10min centrifugation at 12,000g at 4°C, 66µl of the aqueous phase was transferred into a 1.5µl microcentrifuge tube, 156µl of isopropanol [Honeywell #33539] added and the solution thoroughly mixed. After 10min incubation samples were centrifuged for 10min at 12.000g at 4°C and the supernatant was removed. RNA was washed with 250µl 70% ethanol, centrifuged for 2min at 12.000g at 4°C. Ethanol was removed, samples dried, 20µl of nuclease free water [Ambion #AM9930] was added and samples incubated at 45°C for 10min. cDNA was prepared from RNA samples with GoScript reverse transcriptase (Promega) according to manufacture instructions. cDNA was diluted 1:10. Exonic primers for *D. melanogaster PPO3* and *atilla* were designed in NCBI Primer-BLAST online tool: (PPO3_qPCR_2_Fw: 5'-GATGTGGACCGGCCTAACAA-3'; PPO3_qPCR_2_Rev 5'-GATGCCCTTAGCGTCATCCA-3'; atilla_qPCR2_Fw: 5'-ACCCACCAAATATGCTGAAACA-3'; atilla_qPCR2_Rv: TTGATGGCCGATGCACTGT). The gene *RpL32* was used to normalize gene expression (RpL32_qPCR_F-d: 5'-TGCTAAGCTGTCGCACAAATGG-3'; RpL_qPCR_R-h 5'-

550 TGCGCTTGTTCGATCCGTAAC-3'; (Longdon et al., 2015). Sensifast Hi-Rox SyBr kit
551 (Bioline) was used to perform the RT-qPCR on a StepOnePlus system
552 (ThermoFisher Scientific). Each sample was duplicated (qPCR technical replica).
553 The PCR cycle was 95°C for 2min followed by 40 cycles of 95°C for 5s, 60°C for
554 30s.

555

556 **Circulating hemocytes immunohistochemistry, image acquisition and**
557 **analysis**

558 Larvae were prepared in the same conditions as for hemocyte counts, described
559 above. Larvae were washed in $_{dd}H_2O$, dried on filter paper and transferred into a
560 well of multispot porcelain plate with 25µl PBS. Hemolymph was collected by
561 tearing the ventral cuticle with forceps and the hemocyte suspension was
562 transferred into a reaction well of a microscope slide (Marienfeld, #1216330).
563 Samples were incubated for 30min in a humid chamber, fixed for 20 min with
564 3.8% formaldehyde (Sigma-Aldrich #F8775) and washed 3 times with PBS. Cells
565 were blocked and permeabilized with 0.01% Triton-X and 1% NGS diluted in
566 PBS for 30 min and washed 3 times with PBS. Primary antibody against *atilla*
567 (L1, 1:100, (Kurucz et al., 2007)) was added with 1% NGS overnight at 4°C.
568 Primary antibody was washed with PBS for 5 min 3 times and secondary
569 antibody (Alexa Fluor 488, anti-mouse, 1:1000) was applied overnight at 4°C.
570 Cells were washed 3 times with PBS and stained with Hoechst 33342 (Invitrogen
571 #H3570, 1µg/ml) and phalloidin (Alexa Fluor 594, Invitrogen #A12381, dilution
572 1:2000) for 30min. After cells were washed 3 times with PBS, cover slides were
573 mounted with Vectashield (Vector laboratories).

Images were acquired in a Leica DM6000 fluorescence microscope with a 40x objective. Images were analyzed with Fiji version 1.0 (Schindelin et al., 2012). Cells were identified based on actin and nuclear staining and manually outlined with the selection tool. Maximum intensity of *atilla* staining and length of the major axis was recorded for each cell. The threshold for staining intensity was obtained by measuring intensity of cells that were stained following the immunohistochemistry protocol (described above) but with no primary antibody. The threshold for cell size was obtained from a independent set of images where cells were measured and classified as lamellocytes.

Lymph gland immunohistochemistry, image acquisition and analysis

Lymph glands were dissected and processed as previously described (Krzemień et al., 2007). Antibodies used were rabbit anti-αPS4 (1/200) (Krzemień et al., 2007) and mouse anti-β Integrin (Mys) (Developmental Studies Hybridoma Bank, CF.6G11c, 1/100) (Irving et al., 2005). Immunostainings were performed as previously described (Louradour et al., 2017). Nuclei were labeled with DAPI. Optimized stacks were acquired using a Leica SP8 confocal with a 40X immersion objective. Each anterior lymph gland lobe was analyzed manually. When more than 2 cells (Mys^+, □-$PS4^-$) or (Mys^+, $\alpha PS4^+$) were quantified per anterior lobe, the latter was considered as containing immature (Mys^+, $\alpha PS4^-$) or mature (Mys^+,$\alpha PS4^+$) lamellocytes, respectively. The percentage of lymph glands corresponds to the number of anterior lobes having lamellocytes divided by the total number of anterior lobes analyzed. At least 16 anterior lymph gland lobes were analyzed per genotype.

Statistical analysis

All statistical analyses were performed using R. Encapsulation proportions during artificial selection were arcsine transformed and analyzed with a general linear mixed effects model where selection treatment, generation and the interaction term were considered fixed factors and population a random variable. Oil melanization proportions were arcsine transformed and selection regime was used as an explanatory variable in a linear model. To analyze *atilla* and *PPO3* expression from qPCR results we used mixed effects models with treatment, selection regime and the interaction term as fixed effects and population and generation as random variables. Total hemocyte counts and the arcsine transformed lamellocyte proportions were analyzed with mixed effects models with treatment and selection regime as explanatory variables and population as a random variable. Crystal cell counts were analyzed with a linear mixed effects model with selection regime and sex as explanatory variables and population and generation as random variables. The arcsine square root transformed proportions of cells considered atilla^{+} with immunohistochemistry staining were analyzed with a linear model with treatment, selection regime and the interaction term as explanatory variables. The disruption state and presence of immature and mature lamellocytes in lymph gland lobes were analyzed with mixed effects models with treatment and selection regime as explanatory variables and population and larva as random variables. In all cases, significance was assessed with ANOVA.

Hemocyte preparation for scRNAseq

Larvae from both selection regimes and infection treatments were obtained following the protocol for hemocyte counting, as described above. 80 to 140 larvae per biological replica were randomly selected, cleaned in PBS and dried on filter paper. Larvae were transferred into 200µl PBS and dissected by tearing the ventral cuticle. 200µl of hemocyte solution were collected and filtered (Flowmi cell strainer 70µm). The cell suspension was carefully transferred into a 15ml centrifuge tube with OptiPrep solution (Sigma-Aldrich D1556; 540µl OptiPrep and 1460µl PBS). Samples were centrifuged at 170g for 20 min in a swinging bucket centrifuge at 4°C with no brake. The first two layers of 100µl were then carefully removed and hemocytes were counted in a Thoma chamber. The sample fraction with more hemocytes was used for encapsulation in 10X single cell platform at Cancer Research UK Cambridge Institute. Library preparation was performed with standard protocols of single cell 3' V2 chemistry 10X Genomics.

Read alignments and cell detection

Demultiplexed FASTQ data files were aligned to a custom-built *D. melanogaster* reference obtained from FlyBase FB2018_02 Dmel Release 6.21 (Thurmond et al., 2019) and created using the Cell Ranger pipeline (RRID:SCR_017344) (https://support.10xgenomics.com/single-cell-gene-expression/software/overview/welcome, last accessed 23-03-2020). Less than 1,000 cells were detected in libraries generated from control and selected populations in one of the three replicates (replicate two). This replicate was dropped in further analysis. 25,128 cells were identified across the two

remaining replicates. The entire sequence of data filtering and clustering is listed in Figure 3—figure supplement 6. Most of the analyses were done in R versions 3.6 (R Core Team, 2018) and we used the Tidyverse (RRID:SCR_019186), gridExtra and cowplot (RRID:SCR_018081) packages to manipulate and plot the data.

Normalization, integration and dimensionality reduction

Seurat version 3.1.1 (Stuart et al., 2019) (RRID:SCR_007322) was used to process and analyze the single cell count matrix. Unique molecular identifier (UMI) count matrices obtained from Cell Ranger were normalized using a scaling factor of 10,000 and log-normal transformation. 2,000 highly variable genes (HVG) were discovered using the 'vst' method (Supplementary file 7). Count matrices from individual samples were integrated allowing for a maximum of 50 dimensions and 2,000 anchor features.

We identified 281 cells that expressed fewer than 250 features or more than 2,500 features and 5,387 cells that did not express either *He* or *Srp*, two pan-hemocyte markers (Banerjee et al., 2019). These cells were removed from the constituent samples. Following this, the count matrices were normalized, HVG were identified, and the samples were re-integrated.

Mean fold change in gene expression

To combine data across cells to examine gene expression differences between treatments, we performed the data integration steps utilizing all possible

anchors features in Seurat. In doing so, a total of 7,716 genes were used for integrating the sample count matrices (Supplementary file 7). Fold changes in expression between treatments were obtained from the output of *FindMarkers* with min.pct and logfc.threshold both set to 0. The fold change was converted to a $\log_2$ scale and plotted using the R package LSD. We conduced gene ontology (Huang et al., 2009) enrichment analyses on the 173 genes that had at least a 50% change in transcript levels after infection or selection using the Flymine database and tool (Lyne et al., 2007) (RRID:SCR_002694) with the 7,716 genes used as the background list.

Clustering cells from scRNA-seq

Cells were clustered in Seurat. First, expression levels were scaled and percent mitochondria, number of features and UMI count per cell were regressed out. Then, we performed PCA and UMAP dimensionality reductions allowing for 50 dimensions. We did a first round of clustering using the 'pca' reduction and a clustering 'resolution' of 0.2. We identified markers upregulated in each cluster using the function *FindAllMarkers* with 'min.pct' and 'logfc.threshold' both set to 0.25 and tested for differential expression using MAST (Finak et al., 2015). We identified significantly enriched gene ontology categories (Huang et al., 2009) and KEGG (RRID:SCR_012773) and Reactome (RRID:SCR_003485) pathways (Fabregat et al., 2016; Kanehisa et al., 2006) in each cluster using upregulated cluster markers as query and the 2,000 HVG as the background list.

Enrichment analyses from the first round of clustering indicated one cluster, comprising of 28 cells, was highly enriched for male germ cell expressed

693 genes (Supplementary file 8 - cluster 9). These cells were removed from the
694 constituent sample count matrices and the data were re-integrated. In the
695 second round of clustering, a 'resolution' of 0.3 was used and we discovered that
696 cluster 9 (48 cells) and cluster 10 (41 cells) were enriched for genes associated
697 with muscle and fat body tissues, respectively (Supplementary file 9). These cells
698 were removed from the constituent sample count matrices and data were re-
699 integrated. For round three of clustering, a 'resolution' of 0.3 was utilized. At this
700 point, the 19,344 remaining cells were partitioned into nine clusters.

701 We identified the *D. melanogaster* orthologs of human cell cycle markers
702 identified in Tirosh et al. (Tirosh et al., 2016) using the EBI database (Madeira et
703 al., 2019) (RRID:SCR_004727). The expression levels of these cell cycle genes
704 were used to classify cells by phase using the function *CellCycleScoring* in Seurat.
705 Regressing out the difference between the G2M and S phases had a minimal
706 impact on the cell cluster classification for all but one cluster (Supplementary file
707 10). The greater discordance among the lamellocyte cluster CC-5 is due to the
708 placement of cells differentiating along a single lineage into discrete clusters.

709 We tested if using all possible anchors rather than just the highly variable
710 ones had an impact on data integration and clustering. Clustering the data set the
711 7,716 anchors using the same resolution (0.3) largely revealed the same cell
712 clusters save for the appearance of two very small clusters comprising of 113
713 and 56 cells (cluster 9 and 10 - Supplementary file 11). Also, this data set showed
714 that the proportion of lamellocytes (represented by clusters 1,2,4 and 5)
715 increased following high parasitism and infection (Figure 3—figure supplement
716 7) suggesting the choice of anchors did not result in erroneous patterns. When

717 necessary, we converted the Flybase IDs to gene symbols using the org.Dm.eg.db
718 database v.3.7 (Carlson, 2018). The R package reshape2 (Wickham, 2007) was
719 used to estimate proportions of cells in each cluster.

720

721 **Subclustering lamellocytes**

722 We performed subclustering on lamellocytes and their plasmatocyte progenitors
723 to better resolve the trajectory of cell differentiation. Clusters 1, 2, 4 and 5 from
724 round three clustering had enriched expression of described lamellocyte
725 markers (*ItgaPS4*, *atilla*, *mys*, *PPO3* - (Banerjee et al., 2019)) and, therefore, these
726 cells were isolated for subclustering (Figure 3—figure supplement 8A). Cluster 0
727 from round three clustering was identified as the progenitor plasmatocyte
728 population based on the expression of five plasmatocyte markers (*Col4a1*, *Pxn*,
729 *eater*, *Hml*, *NimC1* - (Banerjee et al., 2019)) and three cell cycle markers (*stg* –
730 (Edgar and O'Farrell, 1990), *polo* – (Glover, 2005)and *scra* – (Oegema et al.,
731 2000)) (Figure 3—figure supplement 8B).

732 The presumed lamellocytes and plasmatocyte progenitor were subset
733 from the constituent sample count matrices. The cell count matrices for each
734 sample were normalized and 2,000 HVG were found. Following this,
735 dimensionality reduction and round one of subclustering was performed using a
736 'resolution' parameter of 0.3. In round one of subclustering, we identified 79
737 cells that were significantly enriched for markers representing crystal cells
738 (Figure 3—figure supplement 8C & Supplementary file 12 - cluster 5). These
739 cells were moved to the crystal cell cluster and we did a second round of
740 subclustering on the remaining cells. We followed the same data integration and

741 clustering steps but used a resolution of 0.2. The original cluster identities for
742 lamellocytes and plasmatocyte progenitor cells were replaced with their new
743 identities inferred from the subclustering.

744

745 **Trajectory inference**

746 We used the software Slingshot (Street et al., 2018) (RRID:SCR_017012)
747 to conduct pseudotime analysis. We used all 50 PCA dimensions estimated from
748 Seurat for trajectory inference and ensured lineages were not inferred past
749 endpoints by setting stretch to 0. The cluster with the highest expression of the
750 three cell cycle markers (*stg*, *polo* and *scra*) was set as starting cluster.

751 We identified genes that were differentially expressed between the
752 starting and terminal clusters of lamellocyte differentiation (PLASM1 versus
753 LAM3). We performed gene ontology enrichment on genes with log(e)FC > 1
754 using the *goana* function, part of the R package "limma" (Ritchie et al., 2015)
755 (RRID:SCR_010943) with the 2,000 HVG used as the background list. Gene set
756 enrichment analyses were conducted separately on markers upregulated in the
757 starting (PLASM1) and terminal clusters (LAM3). We removed redundant gene
758 ontology terms using REVIGO (Supek et al., 2011) (RRID:SCR_005825) limiting
759 false discovery rate adjusted P-values to 0.05 and similarity to 0.4. We produced
760 heatmaps of the variable genes belonging to significantly enriched gene ontology
761 categories using a custom modified version of the *DoHeatmap* function from
762 Seurat v3 and grouped genes by mean cluster expression levels. For the
763 heatmap, the log2 fold change gene expression levels were centred on their
764 mean value and divided by their standard deviation. Smaller gene ontology

765 categories whose membership consisted of genes that were wholly part of larger
766 categories were not included in the heatmap plots.

767 The 2,000 HVG were also utilized for identifying lineage markers. A
768 random forest model was fit to identify the genes best able to predict the
769 pseudotime values using R tidymodels. The R package 'Ranger' (Wright and
770 Ziegler, 2017) was used for implementation of the random forest using 2,000
771 trees and a min_n of 15. Variable importance was evaluated by the "altmann" test
772 (Altmann et al., 2010) using 100 permutations. We produced a heatmap of the
773 top 100 lineage markers ranked by variable importance, as described in the
774 preceding section.

775

776 **Cluster definitions**

777 We performed pathway enrichment analyses on all non-lamellocyte clusters
778 with the aim of defining them according to their inferred biological function.
779 First, upregulated cluster markers were identified through pairwise differential
780 expression tests. The cluster of interest was compared with PLASM1 using the
781 function *FindMarkers* with 'min.pct' and 'logfc.threshold' both set to 0.25. Genes
782 with significant upregulation in each cluster were identified using the MAST test
783 statistic (Supplementary file 13) after performing Bonferroni correction on the
784 obtained *P*-values. Markers upregulated in each cluster were used for pathway
785 enrichment analysis. Markers for the plasmatocyte progenitor population were
786 identified through comparisons to the cell types containing other plasmatocyte-
787 type cells. These markers were used for pathway enrichment analyses using the
788 Flymine database and tool (Lyne et al., 2007).

Comparison to other scRNA-seq datasets

We compared our clusters of cells with clusters defined in two published scRNA-seq data sets generated from *D. melanogaster* larval hemocytes. We attained the expression and cell cluster data for Tattikota et al. (2020) from the gene expression omnibus (GEO) repository (RRID:SCR_005012) under accession GSE146596. We attained the expression and cell cluster data for Cattenoz et al. (2020) from the ArrayExpress repository (RRID:SCR_002964) under accession E-MTAB-8698. We used the expression and cluster identity data to create Seurat v3 objects and used Flybase IDs as feature names. For Cattenoz et al. (2020), we combined the the WI and NI data sets into a single object. We normalized the counts, identified 2,000 HVG for each data set and scaled the data using the default options in Seurat v3. We performed a reference-based label transfer using the *FindTransferAnchors* and *TransferData* functions with a 'cca' reduction and L2 normalization. We compared the three data sets in pairs and alternated the reference and query for each comparison. We plot the proportion of cells in query clusters that were predicted to belong to a given reference cluster using the R package 'pheatmap' (RRID:SCR_002630).

References

Altmann A, Toloşi L, Sander O, Lengauer T. 2010. Permutation importance: a corrected feature importance measure. *Bioinformatics* **26**:1340–1347. doi:10.1093/bioinformatics/btq134

813 Anderl I, Vesala L, Ihalainen TO, Vanha-aho LM, Andó I, Rämet M, Hultmark D.
814 2016. Transdifferentiation and Proliferation in Two Distinct Hemocyte
815 Lineages in Drosophila melanogaster Larvae after Wasp Infection. *PLoS*
816 *Pathog* **12**:1–34. doi:10.1371/journal.ppat.1005746

817 Bajgar A, Kucerova K, Jonatova L, Tomcala A, Schneedorferova I, Okrouhlik J,
818 Dolezal T. 2015. Extracellular Adenosine Mediates a Systemic Metabolic
819 Switch during Immune Response. *PLoS Biol* **13**:1–23.
820 doi:10.1371/journal.pbio.1002135

821 Banerjee U, Girard JR, Goins LM, Spratford CM. 2019. *Drosophila* as a Genetic
822 Model for Hematopoiesis. *Genetics* **211**:367–417.
823 doi:10.1534/genetics.118.300223

824 Boots M, Best A. 2018. The evolution of constitutive and induced defences to
825 infectious disease. *Proc R Soc B Biol Sci* **285**. doi:10.1098/rspb.2018.0658

826 Bunt S, Hooley C, Hu N, Scahill C, Weavers H, Skaer H. 2010. Hemocyte-Secreted
827 Type IV Collagen Enhances BMP Signaling to Guide Renal Tubule
828 Morphogenesis in Drosophila. *Dev Cell* **19**:296–306.
829 doi:10.1016/j.devcel.2010.07.019

830 Carlson M. 2018. org.Dm.eg.db: Genome wide annotation for Fly. *R Packag*
831 *version 370* .

832 Cattenoz PB, Sakr R, Pavlidaki A, Delaporte C, Riba A, Molina N, Hariharan N,
833 Mukherjee T, Giangrande A. 2020. Temporal specificity and heterogeneity
834 of Drosophila immune cells . *EMBO J* 1–25. doi:10.15252/embj.2020104486

835 Cho B. 2020. Single-cell transcriptome maps of myeloid blood cell lineages in

836 Drosophila. *bioRxiv*.

837 Cho B, Yoon S-H, Lee D, Koranteng F, Tattikota SG, Cha N, Shin M, Do H, Hu Y, Oh
838 SY, Moon SJ, Perrimon N, Nam J-W, Shim J. 2020. Single-cell transcriptome
839 maps of myeloid blood cell lineages in Drosophila. *bioRxiv*.

840 Dudzic JP, Kondo S, Ueda R, Bergman CM, Lemaitre B. 2015. Drosophila innate
841 immunity: regional and functional specialization of prophenoloxidases. *BMC*
842 *Biol* **13**:81–97. doi:10.1186/s12915-015-0193-6

843 Edgar BA, O'Farrell PH. 1990. The three postblastoderm cell cycles of Drosophila
844 embryogenesis are regulated in G2 by string. *Cell* **62**:469–480.

845 Eslin P, Prevost G. 1998. Hemocyte load and immune resistance to Asobara
846 tabida are correlated in species of the Drosophila melanogaster subgroup. *J*
847 *Insect Physiol* **44**:807–816.

848 Fabregat A, Sidiropoulos K, Garapati P, Gillespie M, Hausmann K, Haw R, Jassal B,
849 Jupe S, Korninger F, McKay S, Matthews L, May B, Milacic M, Rothfels K,
850 Shamovsky V, Webber M, Weiser J, Williams M, Wu G, Stein L, Hermjakob H,
851 D'Eustachio P. 2016. The Reactome pathway Knowledgebase. *Nucleic Acids*
852 *Res* **44**:D481–D487. doi:10.1093/nar/gkv1351

853 Fellowes MD, Kraaijeveld a R, Godfray HC. 1998. Trade-off associated with
854 selection for increased ability to resist parasitoid attack in Drosophila
855 melanogaster. *Proc Biol Sci* **265**:1553–8. doi:10.1098/rspb.1998.0471

856 Finak G, McDavid A, Yajima M, Deng J, Gersuk V, Shalek AK, Slichter CK, Miller
857 HW, McElrath MJ, Prlic M, Linsley PS, Gottardo R. 2015. MAST: a flexible
858 statistical framework for assessing transcriptional changes and

characterizing heterogeneity in single-cell RNA sequencing data. *Genome Biol* **16**:278. doi:10.1186/s13059-015-0844-5

Fu Y, Huang X, Zhang P, Leemput J Van De, Han Z. 2020. Single-cell RNA sequencing identifies novel cell types in Drosophila blood. *J Genet Genomics*. doi:10.1016/j.jgg.2020.02.004

Glover DM. 2005. Polo kinase and progression through M phase in Drosophila: a perspective from the spindle poles. *Oncogene* **24**:230–237. doi:10.1038/sj.onc.1208279

Gopal Tattikota S, Hu Y, Liu Y, Cho B, Barrera V, Steinbaugh M, Yoon S-H, Comjean A, Li F, Dervis F, Hung R-J, Nam J-W, Sui SH, Shim J, Perrimon N. 2020. A single-cell survey of Drosophila blood. *Elife* 1–35. doi:10.1101/2019.12.20.884999

Gopal Tattikota S, Hu Y, Liu Y, Cho B, Barrera V, Steinbaugh M, Yoon S-H, Comjean A, Li F, Dervis F, Hung R-J, Nam J-W, Sui SH, Shim J, Perrimon N. 2019. Preprint: A single-cell survey of Drosophila blood. doi:10.1101/2019.12.20.884999

Graham AL, Allen JE, Read AF. 2005. Evolutionary causes and consequences of immunopathology. *Annu Rev Ecol Evol Syst* **36**:373–397. doi:10.1146/annurev.ecolsys.36.102003.152622

Grigorian M, Mandal L, Hartenstein V. 2011. Hematopoiesis at the onset of metamorphosis: terminal differentiation and dissociation of the Drosophila lymph gland. *Dev Genes Evol*. doi:10.1007/s00427-011-0364-6

Havard S, Eslin P, Prévost G, Doury G. 2009. Encapsulation ability: Are all

Drosophila species equally armed? An investigation in the *obscura* group. *Can J Zool* **87**:635–641. doi:10.1139/Z09-046

Honti V, Csordás G, Kurucz E, Márkus R, Andó I. 2014. The cell-mediated immunity of Drosophila melanogaster: Hemocyte lineages, immune compartments, microanatomy and regulation. *Dev Comp Immunol* 47–56. doi:10.1016/j.dci.2013.06.005

Honti V, Csordás G, Márkus R, Kurucz E, Jankovics F, Andó I. 2010. Cell lineage tracing reveals the plasticity of the hemocyte lineages and of the hematopoietic compartments in Drosophila melanogaster. *Mol Immunol* **47**:1997–2004. doi:10.1016/j.molimm.2010.04.017

Huang DW, Sherman BT, Lempicki RA. 2009. Bioinformatics enrichment tools: paths toward the comprehensive functional analysis of large gene lists. *Nucleic Acids Res* **37**:1–13. doi:10.1093/nar/gkn923

Irving P, Ubeda J, Doucet D, Troxler L, Lagueux M, Zachary D, Hoffmann JA, Hetru C, Meister M. 2005. New insights into Drosophila larval haemocyte functions through genome-wide analysis. *Cell Microbiol* **7**:335–350. doi:10.1111/j.1462-5822.2004.00462.x

Jent D, Perry A, Critchlow J, Tate AT. 2019. Natural variation in the contribution of microbial density to inducible immune dynamics. *Mol Ecol*. doi:10.1111/mec.15293

Kanehisa M, Goto S, Hattori M, Aoki-Kinoshita KF, Itoh M, Kawashima S, Katayama T, Araki M, Hirakawa M. 2006. From genomics to chemical genomics: new developments in KEGG. *Nucleic Acids Res* **34**:D354–D357. doi:10.1093/nar/gkj102

906 Kim-Jo C, Gatti JL, Poirié M. 2019. Drosophila cellular immunity against
907 parasitoid wasps: A complex and time-dependent process. *Front Physiol* **10**.
908 doi:10.3389/fphys.2019.00603

909 Kraaijeveld AR, Godfray HCJ. 1999. Geographic Patterns in the Evolution of
910 Resistance and Virulence in Drosophila and Its Parasitoids. *Am Nat*
911 **153**:S61–S74. doi:10.1086/303212

912 Kraaijeveld AR, Godfray HCJ. 1997. Trade-off between parasitoid resistance and
913 larval competitive ability in Drosophila Melanogaster. *Nature* **389**:278–280.

914 Kraaijeveld AR, Limentani EC, Godfray HC. 2001. Basis of the trade-off between
915 parasitoid resistance and larval competitive ability in Drosophila
916 melanogaster. *Proc Biol Sci* **268**:259–61. doi:10.1098/rspb.2000.1354

917 Krzemień J, Dubois L, Makki R, Meister M, Vincent A, Crozatier M. 2007. Control
918 of blood cell homeostasis in Drosophila larvae by the posterior signalling
919 centre. *Nature* **446**:325–8. doi:10.1038/nature05650

920 Kurucz E, Váczi B, Márkus R, Laurinyecz B, Vilmos P, Zsámboki J, Csorba K, Gateff
921 E, Hultmark D, Andó I. 2007. Definition of Drosophila hemocyte subsets by
922 cell-type specific antigens. *Acta Biol Hung* **58 Suppl**:95–111.
923 doi:10.1556/ABiol.58.2007.Suppl.8

924 Labrosse C, Carton Y, Dubuffet A, Drezen JM, Poirie M. 2003. Active suppression
925 of D. melanogaster immune response by long gland products of the parasitic
926 wasp Leptopilina boulardi. *J Insect Physiol* **49**:513–522. doi:10.1016/S0022-
927 1910(03)00054-4

928 Leitão AB, Bian X, Day JP, Pitton S, Demir E, Jiggins FM. 2019. Independent effects

929 on cellular and humoral immune responses underlie genotype-by-genotype
930 interactions between Drosophila and parasitoids. *PLoS Pathog* **15**:1–13.
931 doi:10.1371/journal.ppat.1008084

932 Lemaitre B, Hoffmann J. 2007. The host defense of Drosophila melanogaster.
933 *Annu Rev Immunol* **25**:697–743.
934 doi:10.1146/annurev.immunol.25.022106.141615

935 Longdon B, Hadfield JD, Day JP, Smith SCL, McGonigle JE, Cogni R, Cao C, Jiggins
936 FM. 2015. The Causes and Consequences of Changes in Virulence following
937 Pathogen Host Shifts. *PLoS Pathog* **11**:1–18.
938 doi:10.1371/journal.ppat.1004728

939 Louradour I, Sharma A, Morin-Poulard I, Letourneau M, Vincent A, Crozatier M,
940 Vanzo N. 2017. Reactive oxygen species-dependent Toll/NF-κB activation in
941 the drosophila hematopoietic niche confers resistance to wasp parasitism.
942 *Elife* **6**:1–22. doi:10.7554/eLife.25496

943 Lyne R, Smith R, Rutherford K, Wakeling M, Varley A, Guillier F, Janssens H, Ji W,
944 Mclaren P, North P, Rana D, Riley T, Sullivan J, Watkins X, Woodbridge M,
945 Lilley K, Russell S, Ashburner M, Mizuguchi K, Micklem G. 2007. FlyMine: an
946 integrated database for Drosophila and Anopheles genomics. *Genome Biol*
947 **8**:R129. doi:10.1186/gb-2007-8-7-r129

948 Madeira F, Park Y mi, Lee J, Buso N, Gur T, Madhusoodanan N, Basutkar P, Tivey
949 ARN, Potter SC, Finn RD, Lopez R. 2019. The EMBL-EBI search and sequence
950 analysis tools APIs in 2019. *Nucleic Acids Res* **47**:W636–W641.
951 doi:10.1093/nar/gkz268

952 Mattila J, Hietakangas V. 2017. Regulation of carbohydrate energy metabolism in

953 Drosophila melanogaster. *Genetics*. doi:10.1534/genetics.117.199885

954 McGonigle JE, Leitão AB, Ommeslag S, Smith S, Day P, Jiggins FM. 2017. Parallel
955 and costly changes to cellular immunity underlie the evolution of parasitoid
956 resistance in three Drosophila species. *PLoS Pathog* **13(10)**:1–20.

957 Nappi AJ, Poirié M, Carton Y. 2009. The Role of Melanization and Cytotoxic By-
958 Products in the Cellular Immune Responses of Drosophila Against Parasitic
959 WaspsAdvances in Parasitology. pp. 99–121.

960 Oegema K, Savoian MS, Mitchison TJ, Field CM. 2000. Functional Analysis of a
961 Human Homologue of the Drosophila Actin Binding Protein Anillin Suggests
962 a Role in Cytokinesis. *J Cell Biol* **150**:539–552. doi:10.1083/jcb.150.3.539

963 Olofsson B, Page DT. 2005. Condensation of the central nervous system in
964 embryonic Drosophila is inhibited by blocking hemocyte migration or
965 neural activity. *Dev Biol* **279**:233–243. doi:10.1016/j.ydbio.2004.12.020

966 Petraki S, Alexander B, Brückner K. 2015. Assaying Blood Cell Populations of the
967 Drosophila melanogaster Larva. *J Vis Exp* 1–11. doi:10.3791/52733

968 Poirié M, Colinet D, Gatti JL. 2014. Insights into function and evolution of
969 parasitoid wasp venoms. *Curr Opin Insect Sci* **6**:52–60.
970 doi:10.1016/j.cois.2014.10.004

971 Poirie M, Frey F, Hita M, Huguet E, Lemeunier F, Periquet G, Carton Y. 2000.
972 Drosophila resistance genes to parasitoids: chromosomal location and
973 linkage analysis. *Proc Biol Sci* **267**:1417–1421. doi:10.1098/rspb.2000.1158

974 R Core Team. 2018. A language and environment for statistical computing. R
975 Foundation for Statistical Computing, Vienna, Austria. *https://wwwR-*

976 *project.org/*.

977 Ritchie ME, Phipson B, Wu D, Hu Y, Law CW, Shi W, Smyth GK. 2015. limma
978 powers differential expression analyses for RNA-sequencing and microarray
979 studies. *Nucleic Acids Res* **43**:e47–e47. doi:10.1093/nar/gkv007

980 Rizki TM. 1957. Alterations in the haemocyte population of Drosophila
981 melanogaster. *J Morphol* **100**:437–458.

982 Rizki TM, Rizki RM. 1994. Parasitoid-Induced Cellular Immune Deficiency in
983 Drosophila. *Ann N Y Acad Sci* **712**:178–194. doi:10.1111/j.1749-
984 6632.1994.tb33572.x

985 Sadd BM, Siva-Jothy MT. 2006. Self-harm caused by an insect's innate immunity.
986 *Proc R Soc B Biol Sci*. doi:10.1098/rspb.2006.3574

987 Salazar-Jaramillo L, Jalvingh KM, Haan A De, Kraaijeveld K, Buermans H. 2017.
988 Inter- and intra-species variation in genome-wide gene expression of
989 Drosophila in response to parasitoid wasp attack. *BMC Genomics* **18**:1–14.
990 doi:10.1186/s12864-017-3697-3

991 Savage HP, Yenson VM, Sawhney SS, Mousseau BJ, Lund FE, Baumgarth N. 2017.
992 Blimp-1-dependent and -independent natural antibody production by B-1
993 and B-1-derived plasma cells. *J Exp Med* **214**:2777–2794.
994 doi:10.1084/jem.20161122

995 Schindelin J, Arganda-Carreras I, Frise E, Kaynig V, Longair M, Pietzsch T,
996 Preibisch S, Rueden C, Saalfeld S, Schmid B, Tinevez J-Y, White DJ,
997 Hartenstein V, Eliceiri K, Tomancak P, Cardona A. 2012. Fiji: an open-source
998 platform for biological-image analysis. *Nat Methods* **9**:676–82.

999 doi:10.1038/nmeth.2019

1000 Shudo E, Iwasa Y. 2001. Inducible defense against pathogens and parasites:
1001 Optimal choice among multiple options. *J Theor Biol* **209**:233–247.
1002 doi:10.1006/jtbi.2000.2259

1003 Sorrentino RP, Carton Y, Govind S. 2002. Cellular immune response to parasite
1004 infection in the Drosophila lymph gland is developmentally regulated. *Dev*
1005 *Biol* **243**:65–80. doi:10.1006/dbio.2001.0542

1006 Street K, Risso D, Fletcher RB, Das D, Ngai J, Yosef N, Purdom E, Dudoit S. 2018.
1007 Slingshot: cell lineage and pseudotime inference for single-cell
1008 transcriptomics. *BMC Genomics* **19**:477. doi:10.1186/s12864-018-4772-0

1009 Stuart T, Butler A, Hoffman P, Hafemeister C, Papalexi E, Mauck WM, Hao Y,
1010 Stoeckius M, Smibert P, Satija R. 2019. Comprehensive Integration of Single-
1011 Cell Data. *Cell* **177**:1888-1902.e21. doi:10.1016/j.cell.2019.05.031

1012 Supek F, Bošnjak M, Škunca N, Šmuc T. 2011. REVIGO Summarizes and Visualizes
1013 Long Lists of Gene Ontology Terms. *PLoS One* **6**:e21800.
1014 doi:10.1371/journal.pone.0021800

1015 Thurmond J, Goodman JL, Strelets VB, Attrill H, Gramates LS, Marygold SJ,
1016 Matthews BB, Millburn G, Antonazzo G, Trovisco V, Kaufman TC, Calvi BR,
1017 Perrimon N, Gelbart SR, Agapite J, Broll K, Crosby L, Santos G dos, Emmert D,
1018 Gramates LS, Falls K, Jenkins V, Matthews B, Sutherland C, Tabone C, Zhou P,
1019 Zytkovicz M, Brown N, Antonazzo G, Attrill H, Garapati P, Holmes A, Larkin
1020 A, Marygold S, Millburn G, Pilgrim C, Trovisco V, Urbano P, Kaufman T, Calvi
1021 B, Czoch B, Goodman J, Strelets V, Thurmond J, Cripps R, Baker P. 2019.
1022 FlyBase 2.0: the next generation. *Nucleic Acids Res* **47**:D759–D765.

1023 doi:10.1093/nar/gky1003

1024 Tirosh I, Izar B, Prakadan SM, Wadsworth MH, Treacy D, Trombetta JJ, Rotem A,
1025 Rodman C, Lian C, Murphy G, Fallahi-Sichani M, Dutton-Regester K, Lin J-R,
1026 Cohen O, Shah P, Lu D, Genshaft AS, Hughes TK, Ziegler CGK, Kazer SW,
1027 Gaillard A, Kolb KE, Villani A-C, Johannessen CM, Andreev AY, Van Allen EM,
1028 Bertagnolli M, Sorger PK, Sullivan RJ, Flaherty KT, Frederick DT, Jane-
1029 Valbuena J, Yoon CH, Rozenblatt-Rosen O, Shalek AK, Regev A, Garraway LA.
1030 2016. Dissecting the multicellular ecosystem of metastatic melanoma by
1031 single-cell RNA-seq. *Science (80-)* **352**:189–196.
1032 doi:10.1126/science.aad0501

1033 Varaldi J, Petit S, Boulétreau M, Fleury F. 2006. The virus infecting the parasitoid
1034 Leptopilina boulardi exerts a specific action on superparasitism behaviour.
1035 *Parasitology* **132**:747–756. doi:10.1017/S0031182006009930

1036 Vivancos RBV, Giangrande A. 1997. glide/gcmIs Expressed and Required in the
1037 Scavenger Cell Lineage. *Dev Biol* **191**:118–130. doi:10.1006/dbio.1997.8702

1038 Wertheim B, Kraaijeveld AR, Hopkins MG, Walther Boer M, Godfray HCJ. 2011.
1039 Functional genomics of the evolution of increased resistance to parasitism
1040 in Drosophila. *Mol Ecol* **20**:932–949. doi:10.1111/j.1365-
1041 294X.2010.04911.x

1042 Westra ER, Van houte S, Oyesiku-Blakemore S, Makin B, Broniewski JM, Best A,
1043 Bondy-Denomy J, Davidson A, Boots M, Buckling A. 2015. Parasite exposure
1044 drives selective evolution of constitutive versus inducible defense. *Curr Biol*
1045 **25**:1043–1049. doi:10.1016/j.cub.2015.01.065

1046 Wickham H. 2007. Reshaping Data with the **reshape** Package. *J Stat Softw* **21**.

doi:10.18637/jss.v021.i12

Wright MN, Ziegler A. 2017. **ranger** : A Fast Implementation of Random Forests for High Dimensional Data in *C++* and *R*. *J Stat Softw* **77**. doi:10.18637/jss.v077.i01

Acknowledgements: The Genomics Core Facility at Cancer Research UK Cambridge Institute, G. Raddi and S. Tattikota provided protocols for the scRNAseq. **Funding:** This work was funded by Natural Environment Research Council grant NE/P00184X/1 to FJ and AL, an EMBO Postdoctoral Fellowship to AL (ALT-1556) and a Natural Sciences and Engineering Research Council of Canada Postdoctoral Fellowship (PDF-516634-2018, Committee: 187) to RA. **Competing Interests:** None. **Data and materials availability:** Unprocessed single cell sequence reads were deposited in the Sequence Read Archive (accession: SRP256887, Bioproject: PRJNA625925) (RRID:SCR_004891). Cell count matrices for all detected genes, cluster identities and processed scRNA-seq results were deposited into GEO (accession: GSE148826) (RRID:SCR_005012). The R script used to analyze the scRNA-seq data is available on Github (Repository: dmel_scRNA_hemocyte) (RRID:SCR_002630).

Figures

Figure 1 Encapsulation rate during selection for parasitoid resistance. (A) Schematic of the experiment (B) The proportion of infected larvae that gave rise to adult flies with visible capsules. An outbred population of *D. melanogaster*

(source, blue square) was used to found six populations that were parasitized every generation with *L. boulardi* (High Parasitism, orange) or maintained without infection (No Parasitism, blue). (C) Proportion of larvae encapsulating oil droplets at generations 33 and 49. Dots represent the proportion calculated from 15-40 injected larvae in triplicate populations from each selection regime. Bar heights represent the mean per selection regime.

Figure 2. Changes in gene expression following selection for resistance and parasitoid infection. (A) Summary of the comparisons shown in the other panels. (B) The change in gene expression following infection in populations maintained without parasitoid infection (x axis) compared to the constitutive gene expression following 26 generations of selection for resistance to the parasitoid wasp *L. boulardi* (y axis). (C) The change in gene expression following infection in populations maintained without parasitoid infection (x axis) compared to the combined induced and constitutive change in gene expression following selection for resistance and infection (y axis). The black diagonals indicate the 1:1 line. The genes *atilla*, *PPO3*, *Trehalase* and *Tret1-1* are highlighted. Colour represents the density of overlain points. Relative expression is expressed as $\log_2$(fold change).

Figure 3. Cell states of *Drosophila melanogaster* larval hemocytes. Two-dimensional UMAP projections and cell state classification. (A) All 19,344 cells combined. PLASM: plasmatocytes; MET: metabolic plasmatocyte cluster; AMP: antimicrobial peptide plasmatocyte cluster; LAM: lamellocytes; CC: crystal cells.

(B) Cells from populations that had undergone 26 generations of selection with no parasitism (top panels) or high parasitism (bottom panels), and were either uninfected (left panels) or 48 hours post infection (right panels). 64-333 million reads were sequenced in each of the eight 10X libraries that we generated (Supplementary file 3). The number of cells detected per library ranged from 787 to 3,463 (Figure 3—figure supplement 4). (C) Proportion of different cell states after infection and selection.

Figure 4. Changes in cell state following infection and adaptation to high rates of parasitism. (A) Trajectory of lamellocyte differentiation. Plasmatocyte progenitors and lamellocytes were subclustered, the trajectories inferred from multi-dimensional principle components analysis, and the lineage projected onto the two-dimensional UMAP plot. (B-C) Log_2 expression levels of *atilla* and *PPO3*. Relative expression levels were estimated from normalized and scaled unique molecular identifier counts. (D) Heatmaps of genes that are upregulated in either the starting or terminal clusters of lamellocyte differentiation and belonging to significantly enriched gene ontology categories (biological function). Log2 fold change gene expression levels were centred on their mean value and divided by their standard deviation.

Figure 5. Changes in circulating and lymph gland hemocytes following infection and adaptation to high parasitism rates. (A) The proportion hemocytes that were morphologically identified as lamellocytes and (B) the concentration of total circulating hemocytes in no infection conditions (light

colors) and 48 hours post infection (dark colors) . Samples were collected from populations that evolved for 34 generation with high parasitism (orange bars) or no parasitism (blue bars) (C) Cell size and atilla expression. The expression of atilla was measured as the fluorescence intensity resulting from immunohistochemistry staining. Cell size was measured along the major axis. Replicated populations from each selection regime are represented by different symbols and the proportion of cells in each quarter of the plot is shown. (D) The proportion of lymph glands from uninfected larvae containing immature lamellocytes (mys^+ α-$PS4^-$) and mature lamellocytes (mys^+ α-$PS4^+$) . (E) Proportion of disrupted lymph glands in uninfected larvae. The lymph gland anterior lobe was considered disrupted when it was either partially or completely disrupted.

Supplementary Figures

Figure 2 — figure supplement 1. Gene expression in circulating hemocytes measured by qPCR *atilla* and *PPO3* expression normalized by the housekeeping gene RpL32 in populations evolved under no parasitism (blue) or high parasitism (orange). Hemocyte samples for RNA extraction were collected from 50-70 larvae 24 hours post infection (dark colors) and from larvae with no infection (light colors). Each dot represents the average ΔCt of two biological replicas per population and lines represent the average per selection regime. *atilla*, Selection regime x Treatment: $\chi2= 15.45$, d.f= 1, $p=8.49x10^{-5}$; *PPO3*, Selection regime x Treatment: $\chi2= 17.64$, d.f= 1, $p=2.67x10^{-5}$

Figure 3—figure supplement 1. Proportions of cells in G1, G2M and S phase in the plasmatocyte, lamellocyte and crystal cell clusters.

Figure 3—figure supplement 2. Expression levels ($\log_e$) of marker genes. A) Relative level of expression of described plasmatocyte and cell cycle genes and B) Relative level of expression most significant marker genes for the plasmatocyte and crystal cell clusters. The MAST test statistic was used to identify significantly upregulated markers in each cluster comparing the cluster of interest with cells in all other clusters. Percent of cells expressing genes are indicated by circle size. C) Distribution of gene expression levels for described lamellocyte genes grouped by cluster identities.

Figure 3—figure supplement 3. Comparison of scRNA-seq data sets from this paper to those from two previously published studies (Cattenoz et al., 2020; Gopal Tattikota et al., 2020). A reference-based label transfer was used to predict cell cluster identity in the query data set. The scale bar indicates the proportion of cells in query clusters (y axis) that are predicted to belong to a given reference cluster (x axis).

Figure 3—figure supplement 4. Number of cells and genes detected, unique molecular identifier count and percent mitochondrial gene expression per cell grouped by sample. HP: high parasitism, NP: No parasitism, I: Infection and NI: no infection. Numbers following HP or NP correspond to replicate.

Figure 3—figure supplement 5. Impact of cell number and library-specific differences on data integration, cell cluster classification and estimating cluster proportions. A) Clustering 8,596 cells from replicate one, B) clustering 10,784 cells from replicate three and C) clustering 6,296 cells where 787 cells were randomly subsampled without replacement in each of eight libraries used for data integration.

Figure 3—figure supplement 6. Flowchart of data filtering and clustering steps. Only cells expressing >250 features and < 2500 features and cells that were either *He*+ or *Srp*+ were kept. Cells expressing high levels of sperm-cell, muscle or fat body marker genes were identified during three rounds of clustering and removed. 19,344 cells remained after filtering. Two rounds of subclustering identified plasmatocyte progenitor and lamellocyte clusters and these identities replaced those attained from round three clustering for relevant cells.

Figure 3—figure supplement 7. Proportion of different cell states after infection and selection following data integration with 7,716 anchors, the maximum number that can be detected.

Figure 3—figure supplement 8. Expression levels ($\log_e$) of marker genes from early rounds of clustering. A) Distribution of gene expression levels of described

lamellocyte marker genes, for clusters identified from round three clustering. B) Relative level of expression of described plasmatocyte and cell cycle marker genes, for clusters identified from round three clustering. C) Relative level of expression of two known crystal cell markers from round one of subclustering, using lamellocytes and their plasmatocyte progenitors. Percent of cells expressing genes are indicated by circle size (B and C).

Figure 4—figure supplement 1. Trajectory of lamellocyte differentiation following subclustering. A) Proportions of cells in G1, G2M and S phase in the plasmatocyte progenitor and lamellocyte clusters. B) Trajectory of lamellocyte differentiation inferred following cell cycle correction and regressing out the difference between the G2M and S phases. Trajectories were inferred from multi-dimensional principle components analysis, and the lineage projected onto the two-dimensional UMAP plot. C) Heatmap of top 100 markers predicting lamellocyte differentiation as ranked by variable importance. Genes are grouped by mean cluster expression level and cells (columns) were ordered by expression of the 101st marker. Log2 fold change gene expression levels were centered on their mean value and divided by their standard deviation.

Figure 5 —figure supplement 1. Changes in number of circulating hemocytes during artificial selection Proportion of lamellocytes (A) and concentration of total circulating hemocytes (B) in population evolved with no parasitism (blue bars) and with high parasitism (orange bars). Samples were collected as late 3rd instar larvae in homeostasis (light colors) or 48 hours post

infection (dark colors). Each dot represents the mean counts of each population calculated from 4-10 replicas and bar height represents the mean of the triplicate lines. Generation 34 is represented in Figure 5A-B.

Figure 5 —figure supplement 2. Hemocyte size and atilla staining intensity in circulating hemocytes. Hemocytes were stained for nuclei (A, hoechst 33342), Actin (A', Phalloidin- Alexa594) and atilla (A'', L1 antibody + Alexa488). Composite images were created for phallodin and hoechst staining to identify cells with selection tool (yellow line) and fluorescence intensity was measured in L1 staining.

Figure 5 – figure supplementary 3: Lamellocytes differentiation state and morphology of anterior lymph gland lobes (a) Anterior lobe of a lymph gland from a larva from No Parasitism selection regime. Immature lamellocytes are stained with Myspheroid (Mys, green, with arrow). Mature lamellocytes are double stained with Mys and Integrin alpha PS4 subunit (α-PS4, red, white dotted arrow). (b,c) No Parasitism anterior lobe in mild larval stage 3; normal (b) and disrupted lobe (c). (d,e) High Parasitism anterior lobe in mild larval stage 3; normal (d) and disrupted lobe (e). (f,g) No Parasitism anterior lobe in late larval stage 3; normal (f) and disrupted (g). (h,i) High Parasitism anterior lobe in late larval stage 3; normal (i) and disrupted (j). All samples were stained with Mys (green), α-PS4 (red). Nuclei were stained with DAPI. Scale bars=20μm.

Figure 5 —figure supplement 4. Hemocyte concentrations during development of 3rd instar larvae. Total number of hemocytes (A), lamellocytes (B) and lamellocyte proportions (C) in larvae 12, 24, 36 and 48 hours post infection (dark colors) and corresponding controls with no infection (light colors). Points represent the mean of three biological replicas from each triplicate line of No Parasitism (blue) and High Parasitism (orange) selection regimes. Restrictions on working hours mean the 12h and 36h timepoints were performed separately to the 24h and 48h timepoints.

Figure 5 —figure supplement 5. Effect of selection in circulating hemocytes and sessile hemocytes. Concentration of hemocytes from dissected larvae without manipulation (Circulating) and after vortexing to displace sessile hemocytes into circulation (Circulating + Sessile). Points represent the mean of four biological replicas for each triplicate line from populations evolved with No Parasitism (blue) and High Parasitism (orange) selection regimes. Bar heights represent the mean of triplicate lines.

Figure 5 —figure supplement 6. Sessile crystal cells numbers. Number of sessile crystal cells in dorsal side of the A7 abdominal segment of larvae in male and female larvae. Dots represent the average number of crystal cells calculated from 10 larvae of each triplicate population from both selection regimes. Bar heights represent the average of each selection regime, No Parasitism (Blue) and High Parasitism (Orage).

1260

Supplementary Files

Supplementary file 1. Gene ontology enrichment for 173 genes that had > 50% change in transcript levels after infection or selection.

Supplementary file 2. Enriched gene ontology categories and pathways for non-lamellocyte clusters.

Supplementary file 3. 10x v2 library sequencing metrics.

Supplementary file 4. Lamellocyte lineage classification with and without cell cycle correction.

Supplementary file 5. List of marker genes for predicting lamellocyte differentiation.

Supplementary file 6. Enriched gene ontology categories and pathways for lamellocytes.

Supplementary file 7. Genes detected in scRNA-seq dataset.

Supplementary file 8. Cluster markers identified from round one of clustering.

Supplementary file 9. Cluster markers identified from round two of clustering.

Supplementary file 10. Hemocyte classification with and without cell cycle correction.

Supplementary file 11. Hemocyte classification using 2,000 highly variable genes or all 7,716 detected genes.

Supplementary file 12. Cluster markers identified from round one of subclustering.

Supplementary file 13. Marker genes for non-lamellocyte clusters.

Source Data Files

Figure 1—source data 1.

Figure 2—source data 1. Log2 fold change in gene expression following selection and/or infection with parasitoid wasp *L. boulardi*.

Figure 4—source data 1.

Figure 5—source data 1.

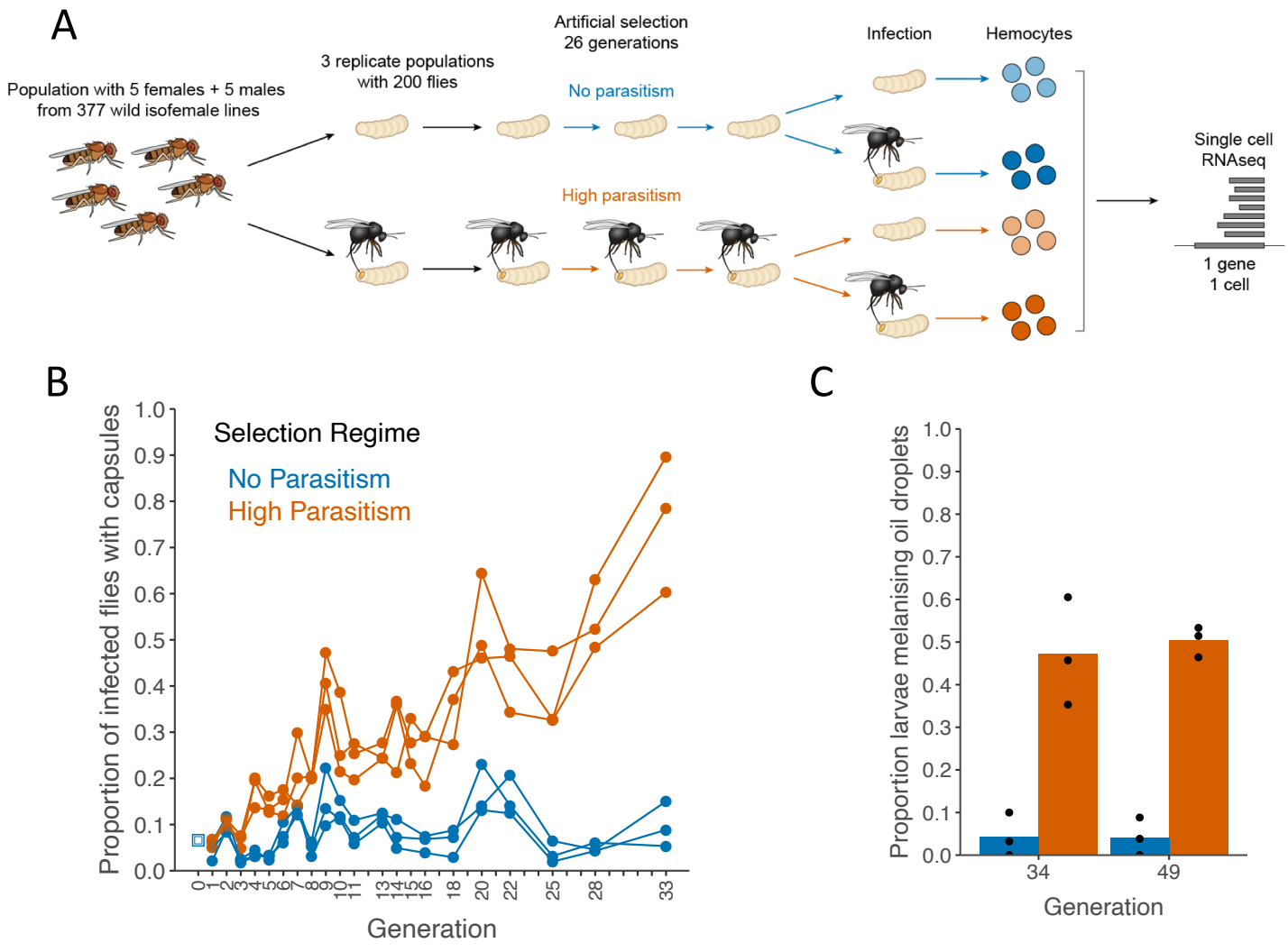
A
Population with 5 females + 5 males
from 377 wild isofemale lines
3 replicate populations
with 200 flies
Artificial selection
26 generations
No parasitism
High parasitism
Infection
Hemocytes
Single cell
RNAseq
1 gene
1 cell
B
Selection Regime
No Parasitism
High Parasitism
Proportion of infected flies with capsules
Generation
C
Proportion larvae melanising oil droplets
Generation

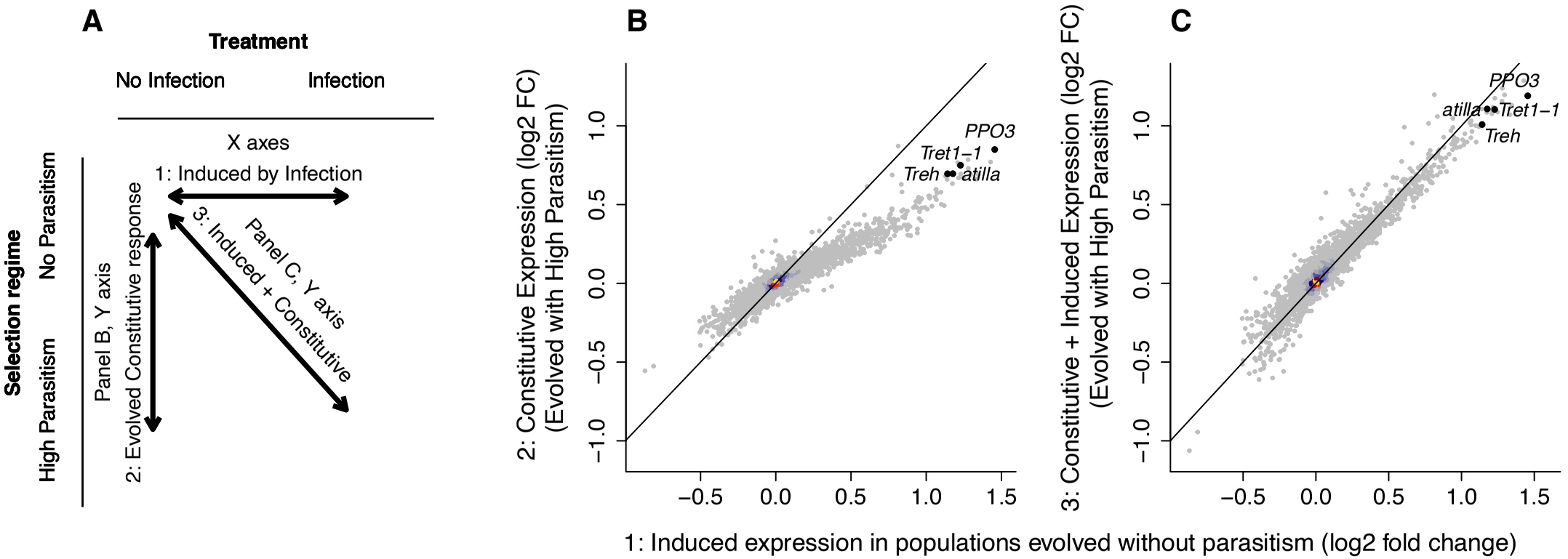
A
Treatment
No Infection
Infection
X axes
1: Induced by Infection
Selection regime
No Parasitism
High Parasitism
Panel B, Y axis
2: Evolved Constitutive response
3: Induced + Constitutive
Panel C, Y axis
B
2: Constitutive Expression (log2 FC)
(Evolved with High Parasitism)
PPO3
Tret1−1
Treh
atilla
−1.0
−0.5
0.0
0.5
1.0
1.5
C
3: Constitutive + Induced Expression (log2 FC)
(Evolved with High Parasitism)
PPO3
atilla
Tret1−1
Treh
1: Induced expression in populations evolved without parasitism (log2 fold change)

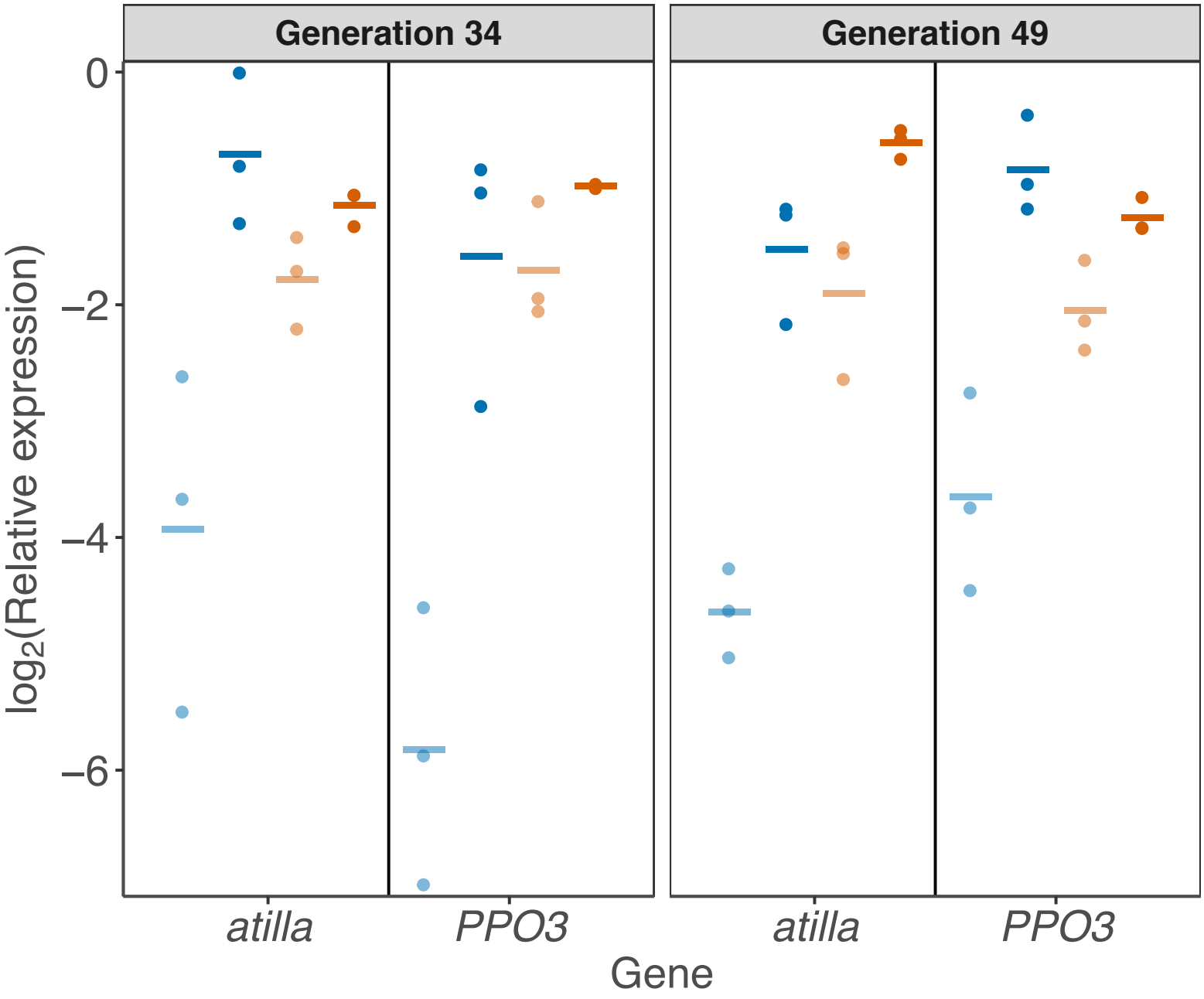
Generation 34
Generation 49
0
−2
−4
−6
log2(Relative expression)
atilla
PPO3
atilla
PPO3
Gene

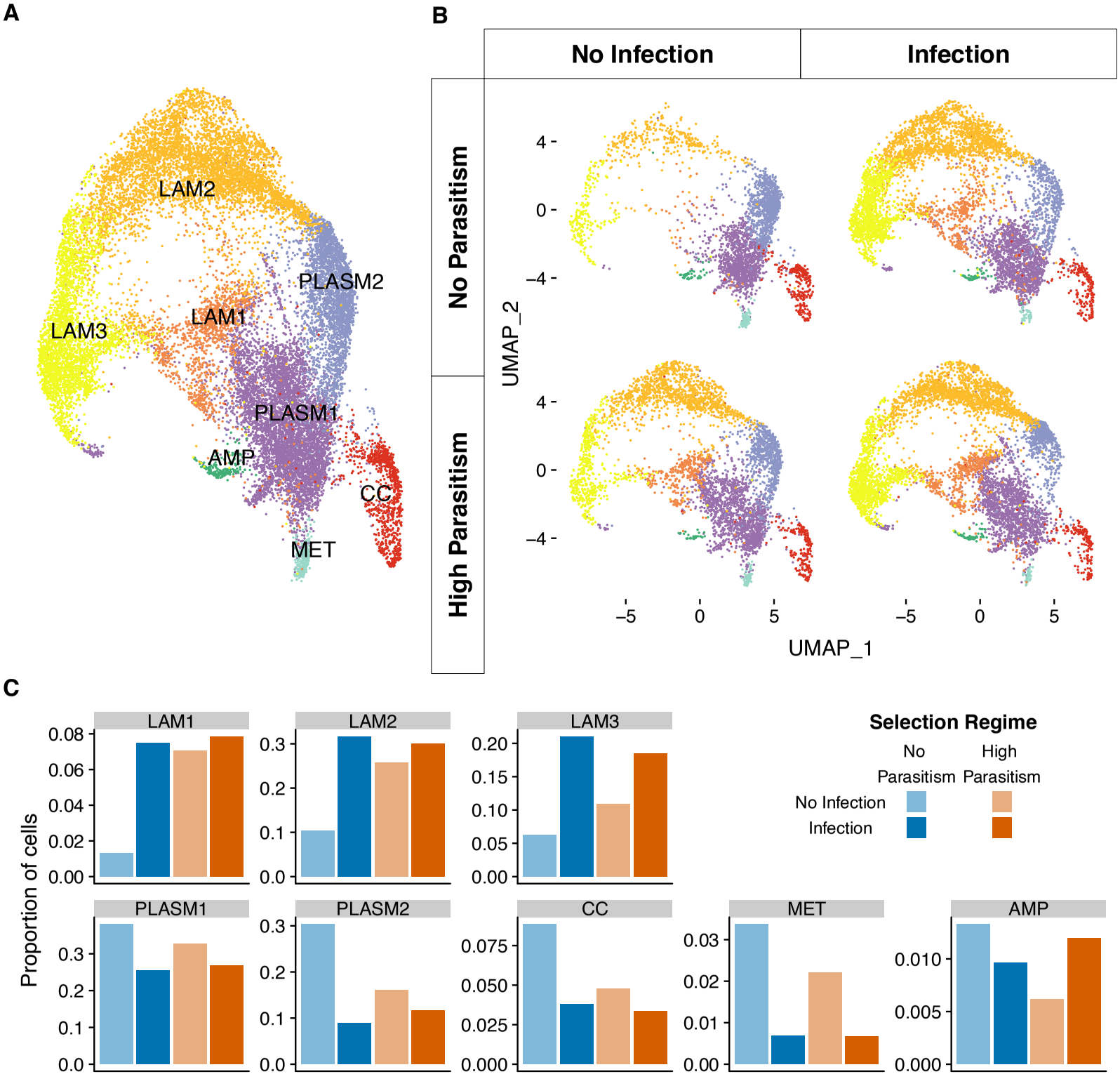
A
LAM2
PLASM2
LAM1
LAM3
PLASM1
AMP
CC
MET
B
No Infection
Infection
No Parasitism
High Parasitism
UMAP_2
UMAP_1
C
LAM1
LAM2
LAM3
PLASM1
PLASM2
CC
MET
AMP
Proportion of cells
Selection Regime
No Parasitism
High Parasitism
No Infection
Infection

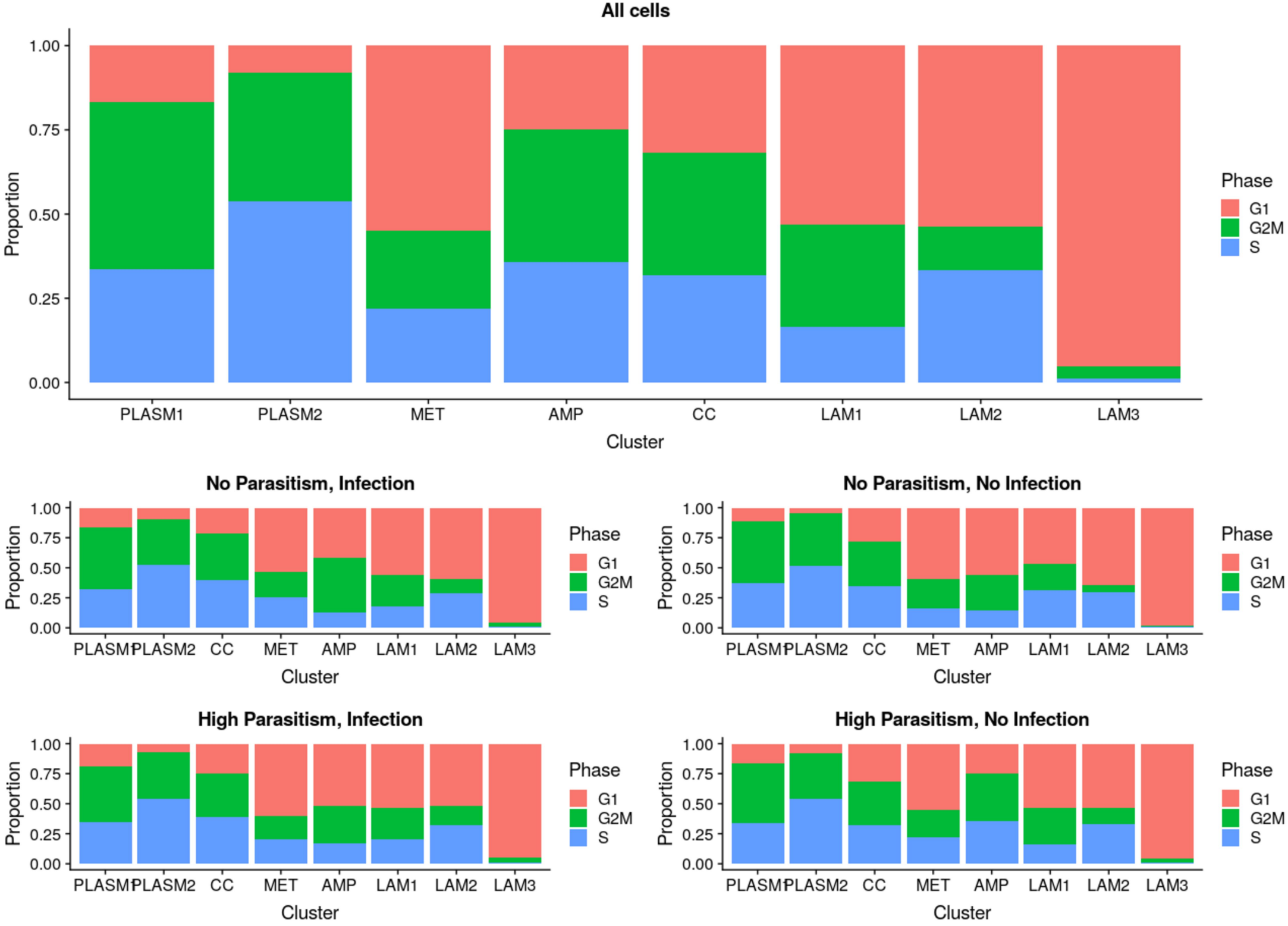
All cells
Proportion
1.00
0.75
0.50
0.25
0.00
PLASM1
PLASM2
MET
AMP
CC
LAM1
LAM2
LAM3
Cluster
Phase
G1
G2M
S
No Parasitism, Infection
No Parasitism, No Infection
High Parasitism, Infection
High Parasitism, No Infection

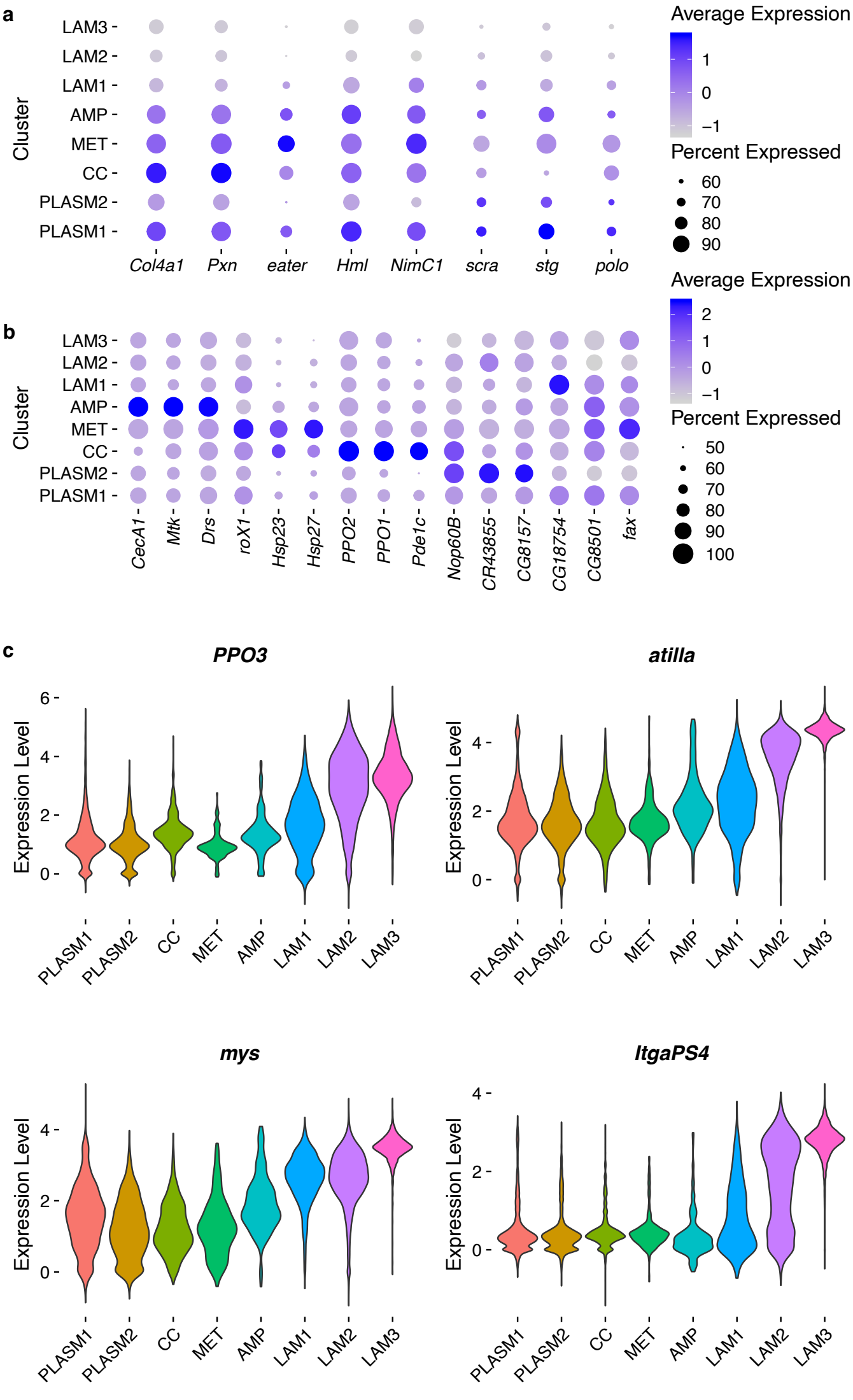
a
Cluster
LAM3
LAM2
LAM1
AMP
MET
CC
PLASM2
PLASM1
Col4a1
Pxn
eater
Hml
NimC1
scra
stg
polo
Average Expression
1
0
−1
Percent Expressed
60
70
80
90
b
Cluster
CecA1
Mtk
Drs
roX1
Hsp23
Hsp27
PPO2
PPO1
Pde1c
Nop60B
CR43855
CG8157
CG18754
CG8501
fax
Average Expression
2
1
0
−1
Percent Expressed
50
60
70
80
90
100
c
PPO3
atilla
mys
ItgaPS4
Expression Level
PLASM1
PLASM2
CC
MET
AMP
LAM1
LAM2
LAM3

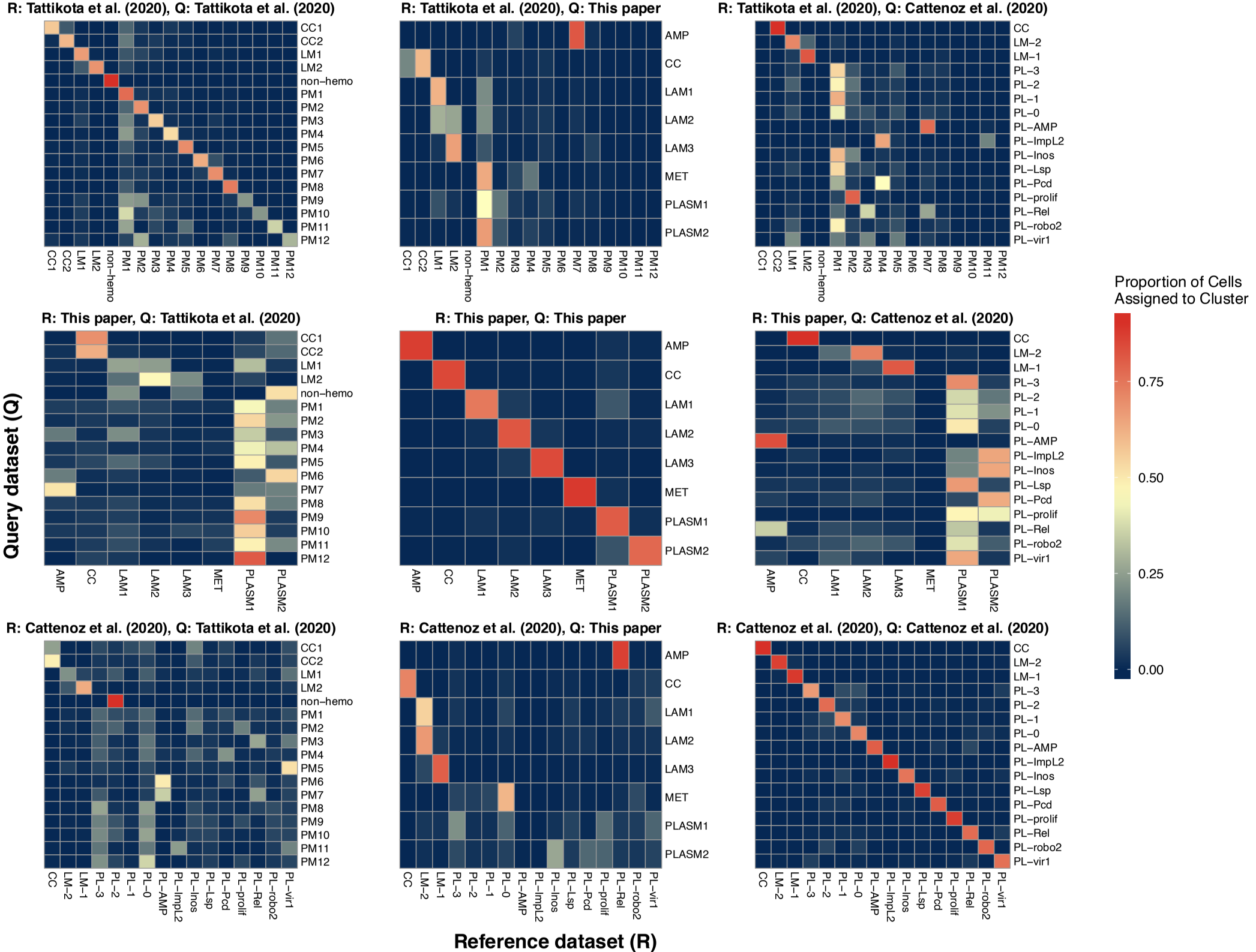
R: Tattikota et al. (2020), Q: Tattikota et al. (2020)
R: Tattikota et al. (2020), Q: This paper
R: Tattikota et al. (2020), Q: Cattenoz et al. (2020)
R: This paper, Q: Tattikota et al. (2020)
R: This paper, Q: This paper
R: This paper, Q: Cattenoz et al. (2020)
R: Cattenoz et al. (2020), Q: Tattikota et al. (2020)
R: Cattenoz et al. (2020), Q: This paper
R: Cattenoz et al. (2020), Q: Cattenoz et al. (2020)
Query dataset (Q)
Reference dataset (R)
Proportion of Cells Assigned to Cluster
0.00
0.25
0.50
0.75
CC1 CC2 LM1 LM2 non–hemo PM1 PM2 PM3 PM4 PM5 PM6 PM7 PM8 PM9 PM10 PM11 PM12
AMP CC LAM1 LAM2 LAM3 MET PLASM1 PLASM2
CC LM–2 LM–1 PL–3 PL–2 PL–1 PL–0 PL–AMP PL–ImpL2 PL–Inos PL–Lsp PL–Pcd PL–prolif PL–Rel PL–robo2 PL–vir1

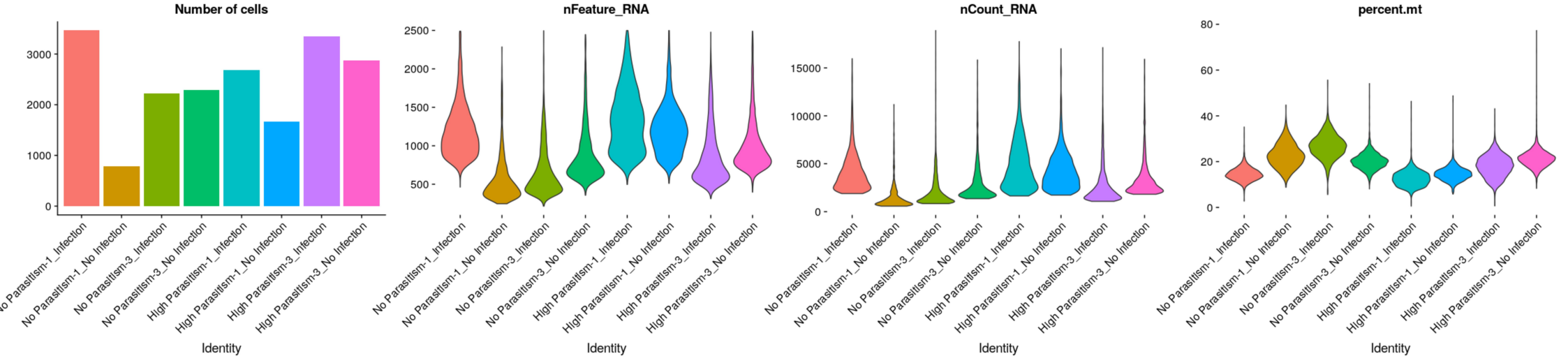
Number of cells
3000
2000
1000
0
No Parasitism-1_Infection
No Parasitism-1_No Infection
No Parasitism-3_Infection
No Parasitism-3_No Infection
High Parasitism-1_Infection
High Parasitism-1_No Infection
High Parasitism-3_Infection
High Parasitism-3_No Infection
Identity
nFeature_RNA
2500
2000
1500
1000
500
Identity
nCount_RNA
15000
10000
5000
0
Identity
percent.mt
80
60
40
20
0
Identity

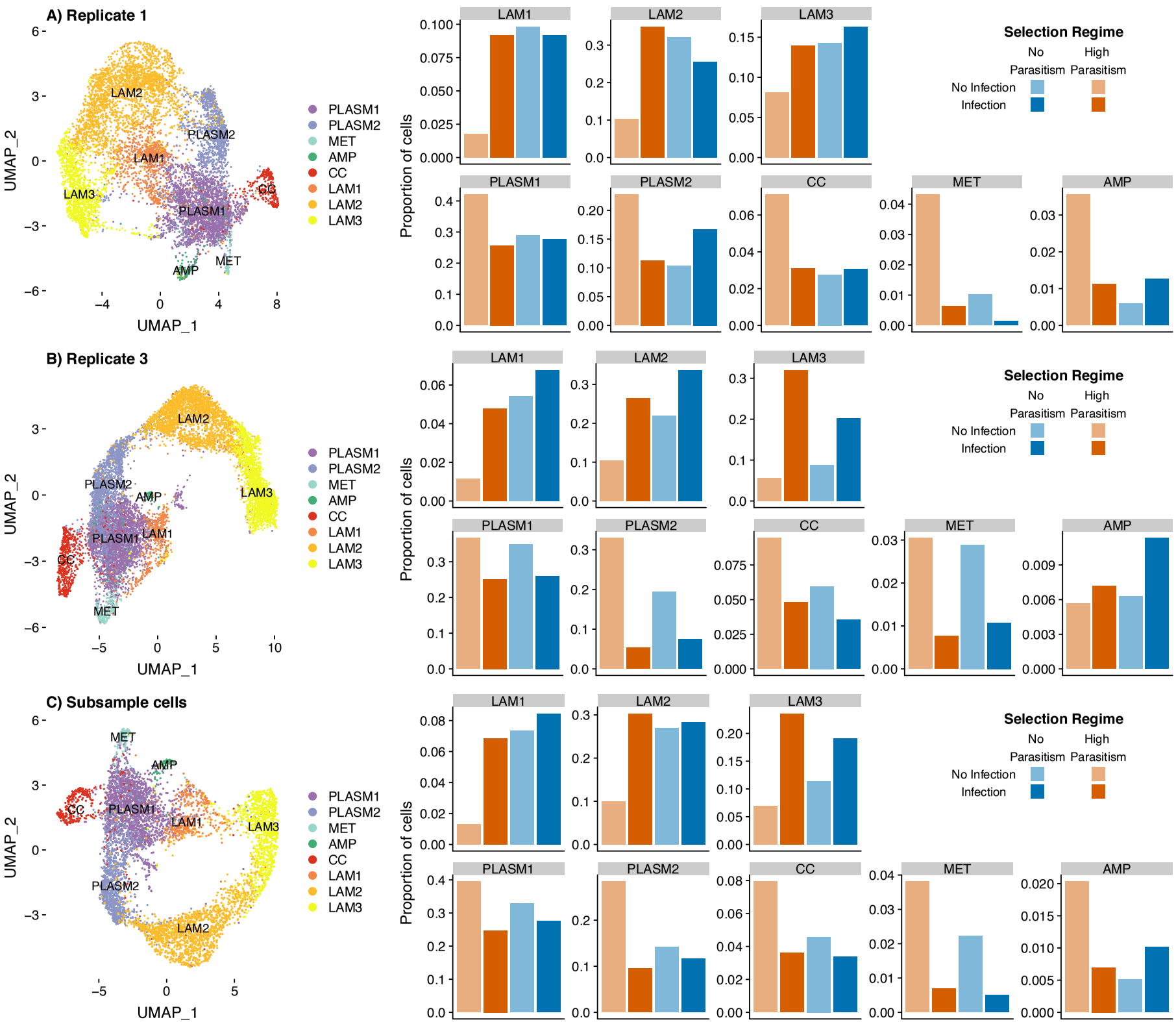
A) Replicate 1
B) Replicate 3
C) Subsample cells
UMAP_1
UMAP_2
PLASM1
PLASM2
MET
AMP
CC
LAM1
LAM2
LAM3
Proportion of cells
Selection Regime
No Parasitism
High Parasitism
No Infection
Infection

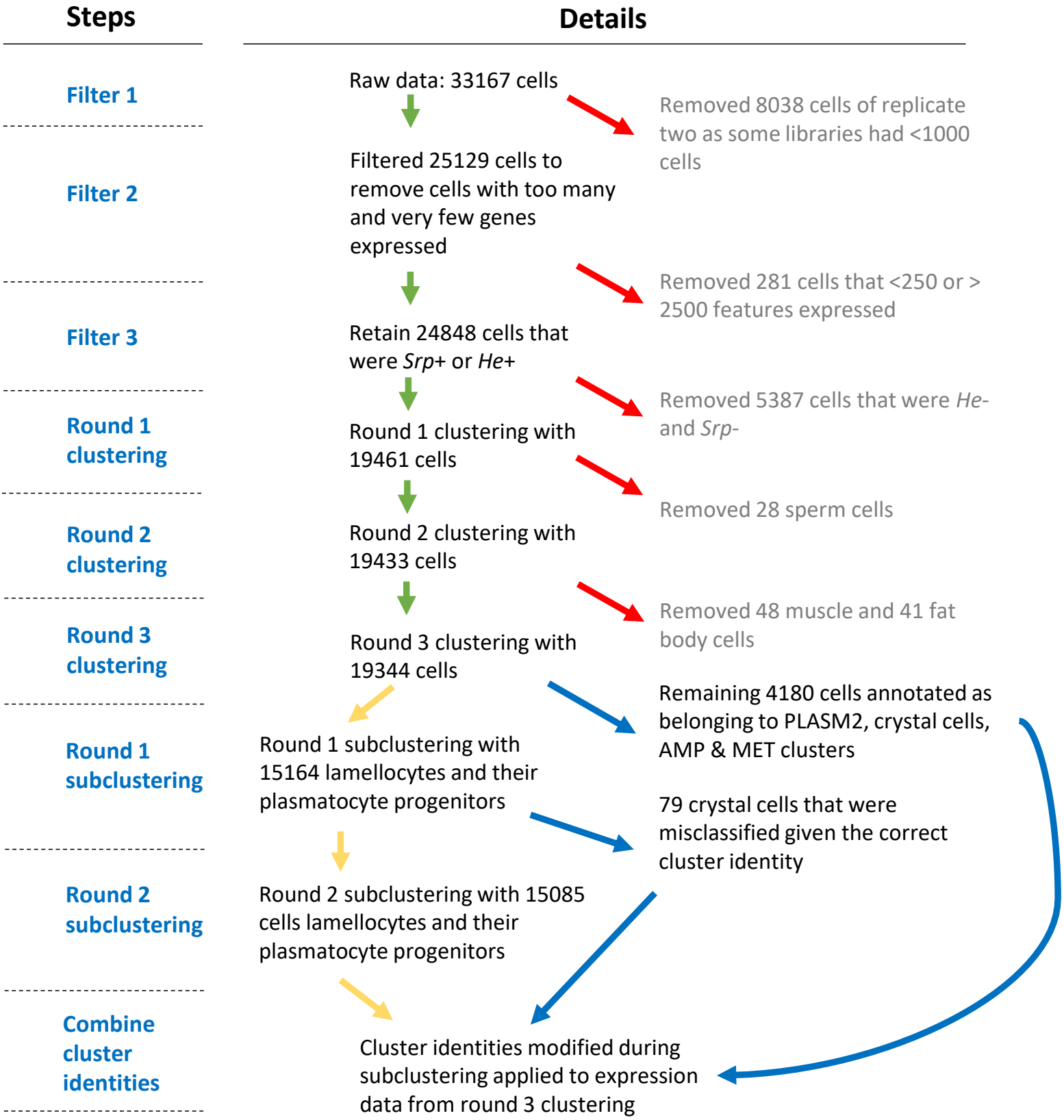
Steps
Details
Filter 1
Filter 2
Filter 3
Round 1 clustering
Round 2 clustering
Round 3 clustering
Round 1 subclustering
Round 2 subclustering
Combine cluster identities
Raw data: 33167 cells
Removed 8038 cells of replicate two as some libraries had <1000 cells
Filtered 25129 cells to remove cells with too many and very few genes expressed
Removed 281 cells that <250 or > 2500 features expressed
Retain 24848 cells that were Srp+ or He+
Removed 5387 cells that were He- and Srp-
Round 1 clustering with 19461 cells
Removed 28 sperm cells
Round 2 clustering with 19433 cells
Removed 48 muscle and 41 fat body cells
Round 3 clustering with 19344 cells
Remaining 4180 cells annotated as belonging to PLASM2, crystal cells, AMP & MET clusters
Round 1 subclustering with 15164 lamellocytes and their plasmatocyte progenitors
79 crystal cells that were misclassified given the correct cluster identity
Round 2 subclustering with 15085 cells lamellocytes and their plasmatocyte progenitors
Cluster identities modified during subclustering applied to expression data from round 3 clustering

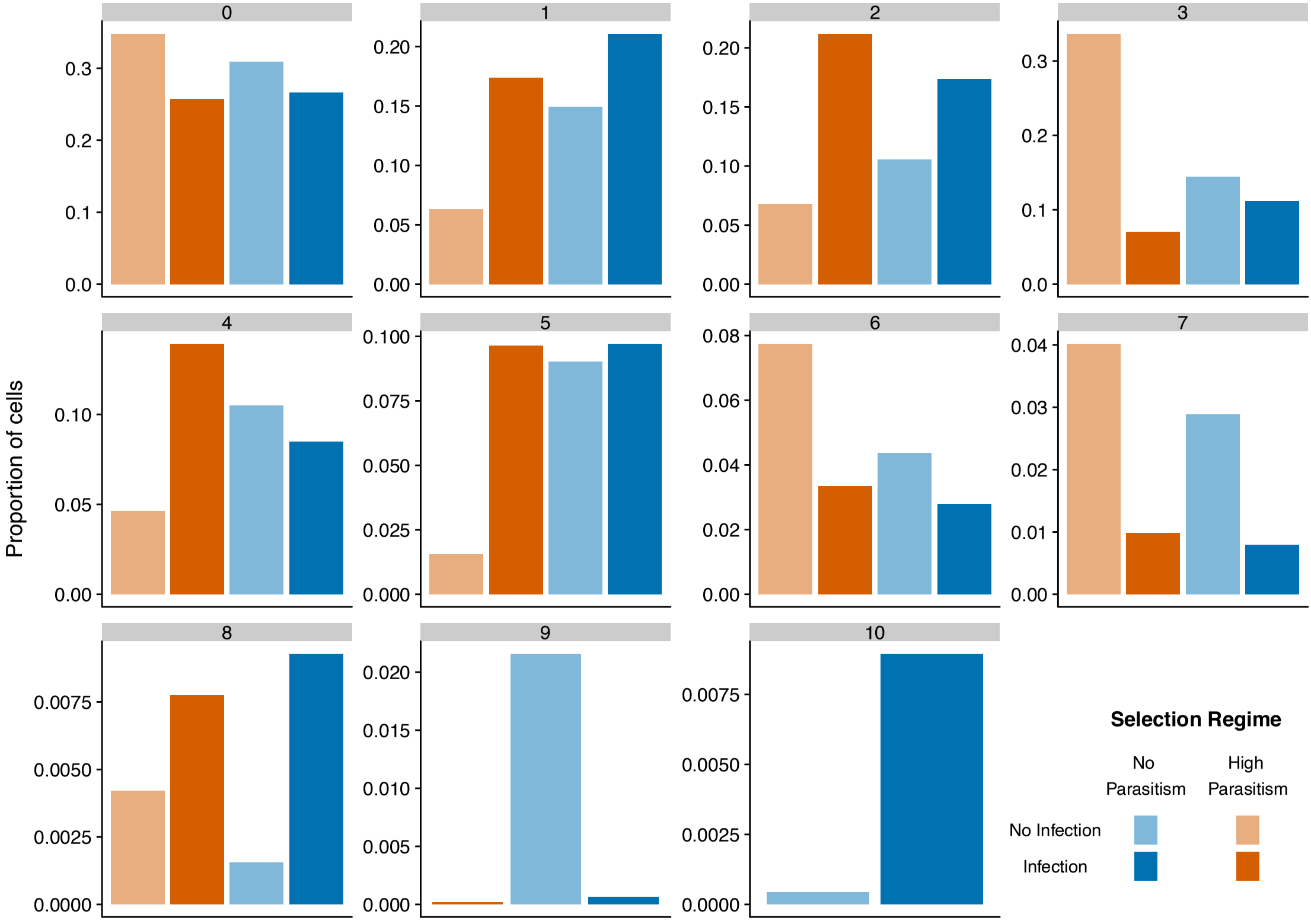
0
1
2
3
4
5
6
7
8
9
10
Proportion of cells
Selection Regime
No Parasitism
High Parasitism
No Infection
Infection

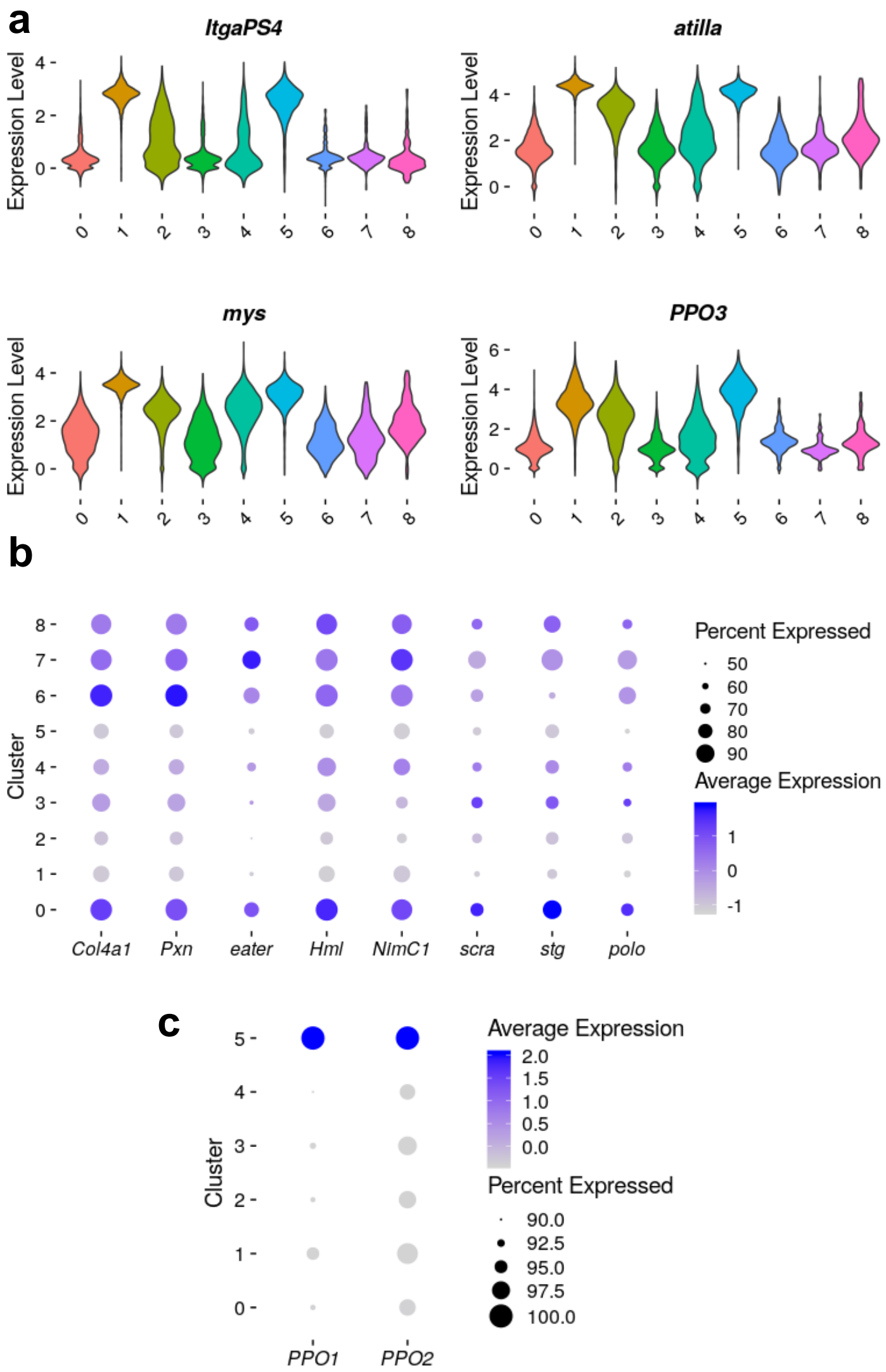
a
ItgaPS4
atilla
mys
PPO3
Expression Level
b
Cluster
Col4a1
Pxn
eater
Hml
NimC1
scra
stg
polo
Percent Expressed
Average Expression
c
PPO1
PPO2

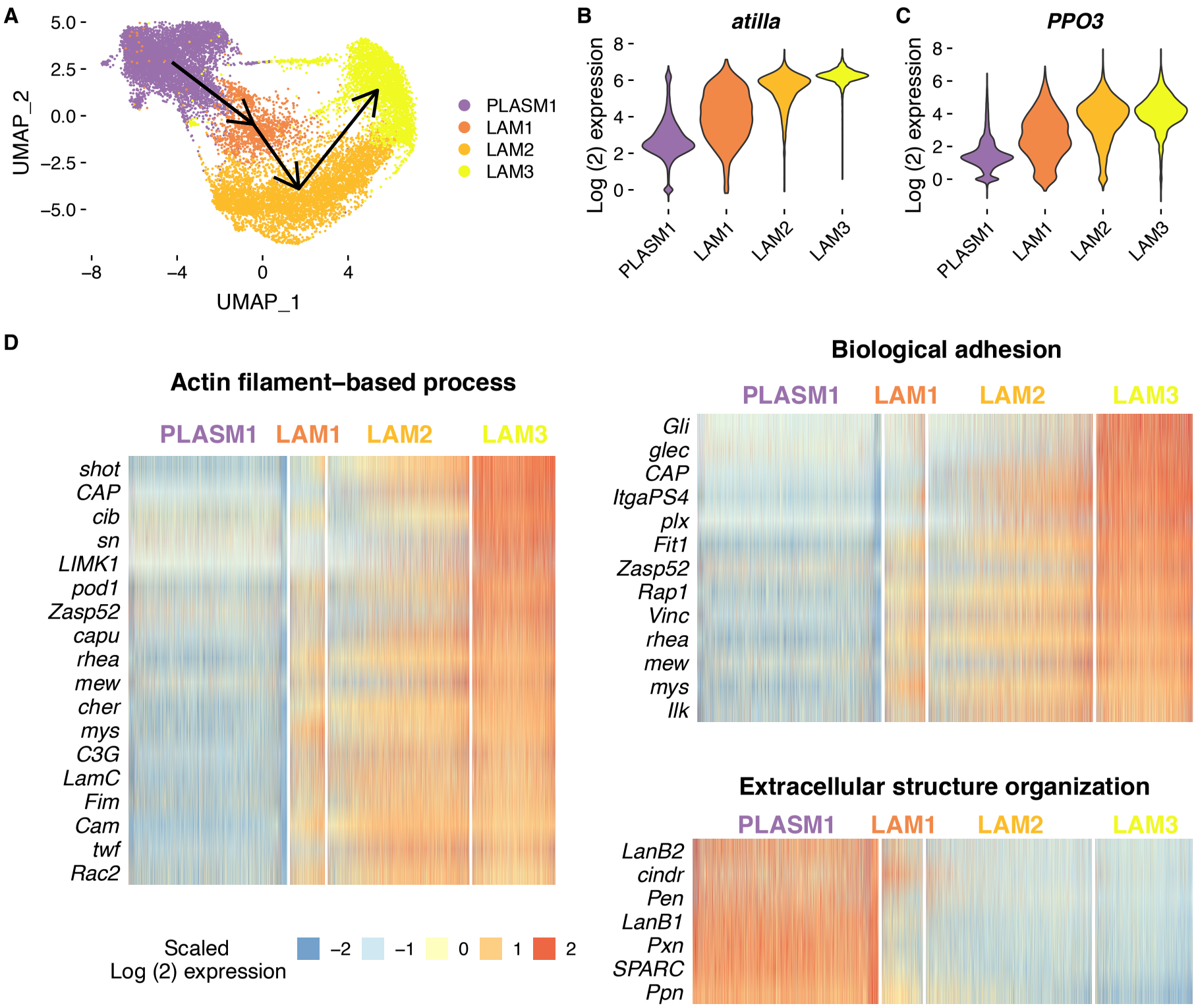
A
UMAP_2
UMAP_1
PLASM1
LAM1
LAM2
LAM3
B
atilla
Log (2) expression
C
PPO3
Log (2) expression
D
Actin filament–based process
Biological adhesion
Extracellular structure organization
shot
CAP
cib
sn
LIMK1
pod1
Zasp52
capu
rhea
mew
cher
mys
C3G
LamC
Fim
Cam
twf
Rac2
Gli
glec
CAP
ItgaPS4
plx
Fit1
Zasp52
Rap1
Vinc
rhea
mew
mys
Ilk
LanB2
cindr
Pen
LanB1
Pxn
SPARC
Ppn
Scaled
Log (2) expression

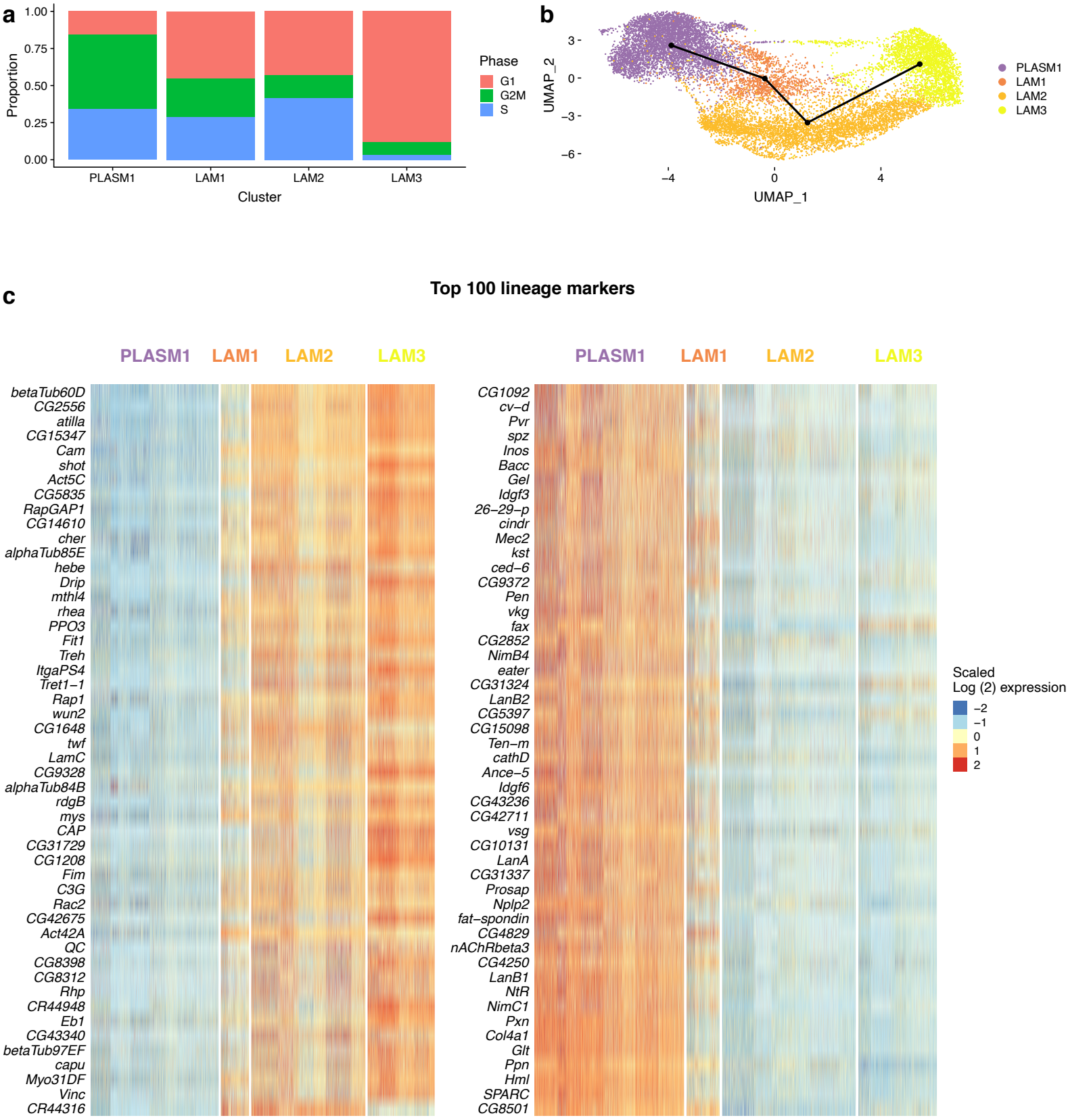
a
1.00
0.75
0.50
0.25
0.00
Proportion
PLASM1
LAM1
LAM2
LAM3
Cluster
Phase
G1
G2M
S
b
3
0
−3
−6
UMAP_2
−4
0
4
UMAP_1
PLASM1
LAM1
LAM2
LAM3
c
Top 100 lineage markers
PLASM1
LAM1
LAM2
LAM3
betaTub60D
CG2556
atilla
CG15347
Cam
shot
Act5C
CG5835
RapGAP1
CG14610
cher
alphaTub85E
hebe
Drip
mthl4
rhea
PPO3
Fit1
Treh
ItgaPS4
Tret1−1
Rap1
wun2
CG1648
twf
LamC
CG9328
alphaTub84B
rdgB
mys
CAP
CG31729
CG1208
Fim
C3G
Rac2
CG42675
Act42A
QC
CG8398
CG8312
Rhp
CR44948
Eb1
CG43340
betaTub97EF
capu
Myo31DF
Vinc
CR44316
PLASM1
LAM1
LAM2
LAM3
CG1092
cv−d
Pvr
spz
Inos
Bacc
Gel
Idgf3
26−29−p
cindr
Mec2
kst
ced−6
CG9372
Pen
vkg
fax
CG2852
NimB4
eater
CG31324
LanB2
CG5397
CG15098
Ten−m
cathD
Ance−5
Idgf6
CG43236
CG42711
vsg
CG10131
LanA
CG31337
Prosap
Nplp2
fat−spondin
CG4829
nAChRbeta3
CG4250
LanB1
NtR
NimC1
Pxn
Col4a1
Glt
Ppn
Hml
SPARC
CG8501
Scaled
Log (2) expression
−2
−1
0
1
2

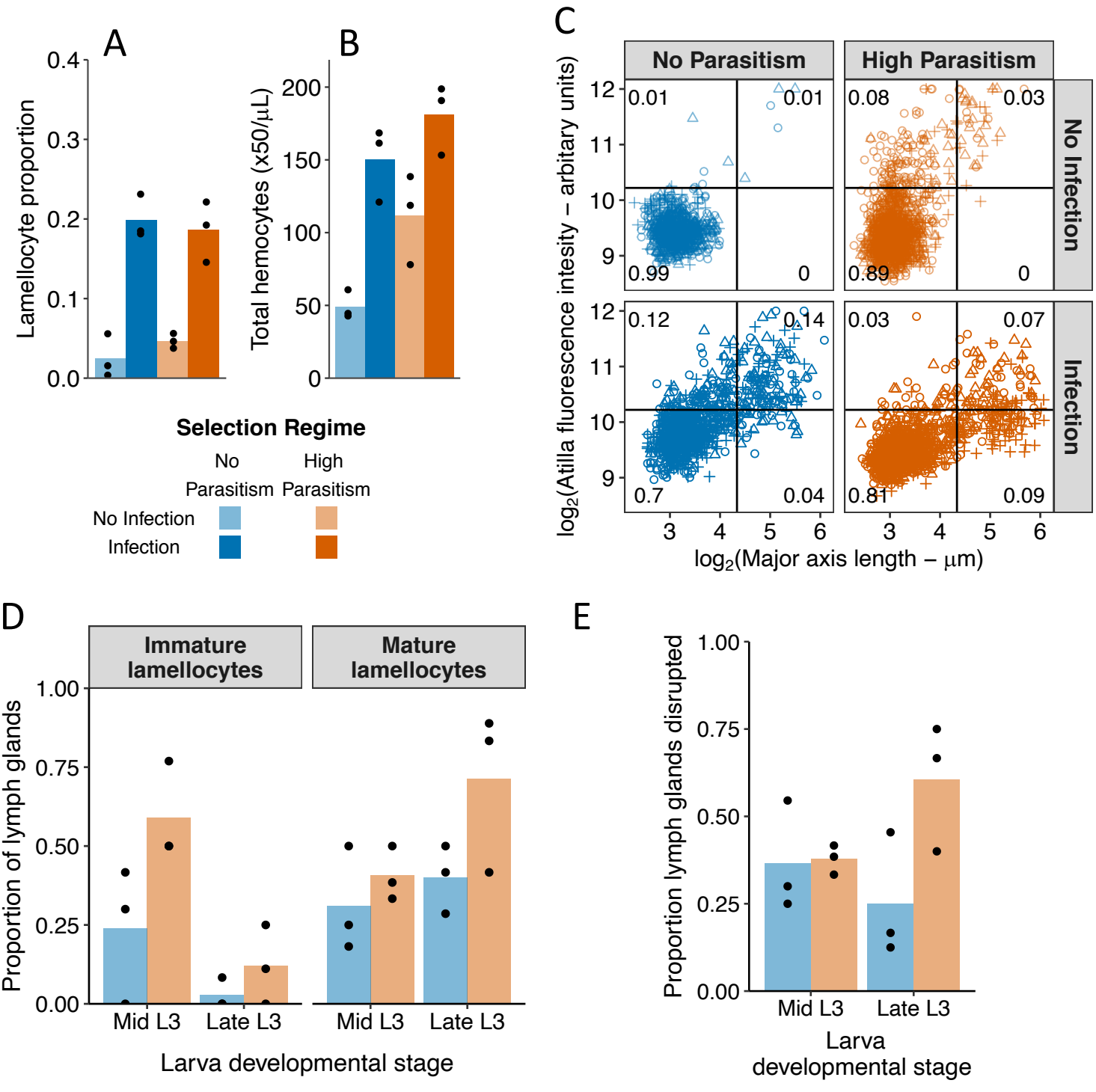
A
B
C
D
E
Lamellocyte proportion
Total hemocytes (x50/µL)
Selection Regime
No Parasitism
High Parasitism
No Infection
Infection
No Parasitism
High Parasitism
No Infection
Infection
log2(Atilla fluorescence intesity – arbitary units)
log2(Major axis length – µm)
0.01
0.01
0.99
0
0.08
0.03
0.89
0
0.12
0.14
0.7
0.04
0.03
0.07
0.81
0.09
Immature lamellocytes
Mature lamellocytes
Proportion of lymph glands
Mid L3
Late L3
Larva developmental stage
Proportion lymph glands disrupted
Mid L3
Late L3
Larva developmental stage

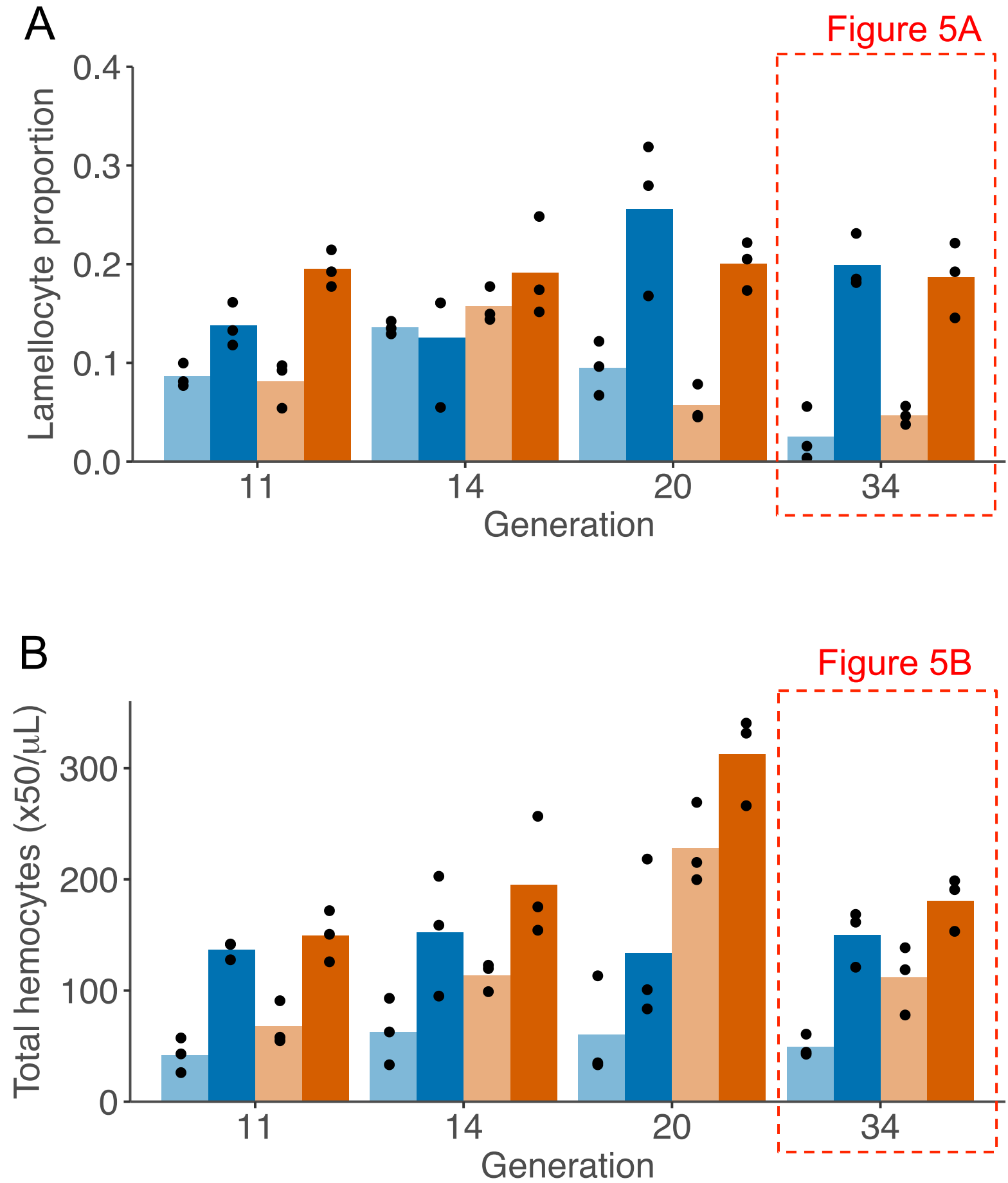
A
Figure 5A
Lamellocyte proportion
0.4
0.3
0.2
0.1
0.0
11
14
20
34
Generation
B
Figure 5B
Total hemocytes (x50/µL)
300
200
100
0
11
14
20
34
Generation

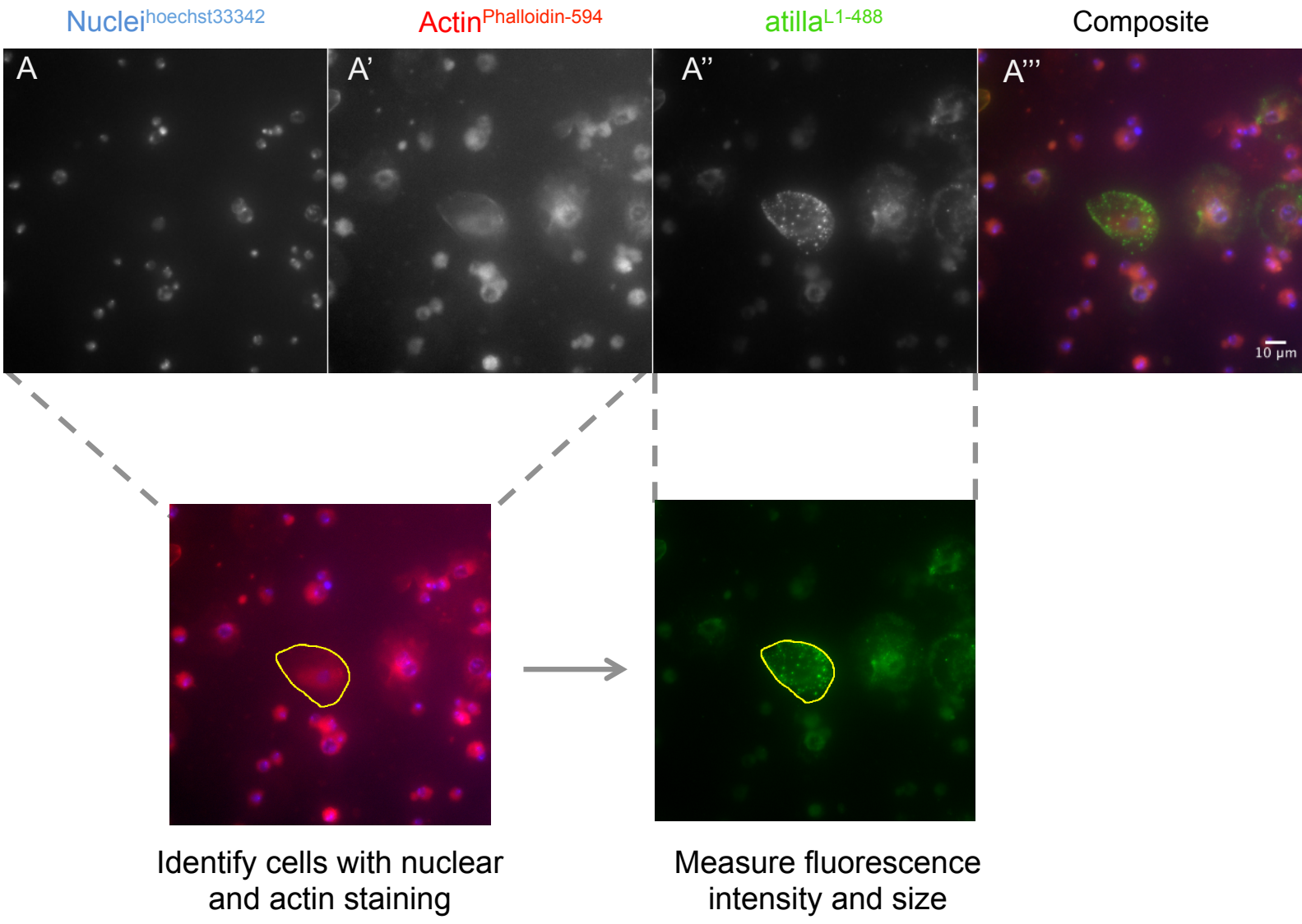
Nuclei hoechst33342
Actin Phalloidin-594
atilla L1-488
Composite
A
A'
A''
A'''
10 µm
Identify cells with nuclear and actin staining
Measure fluorescence intensity and size

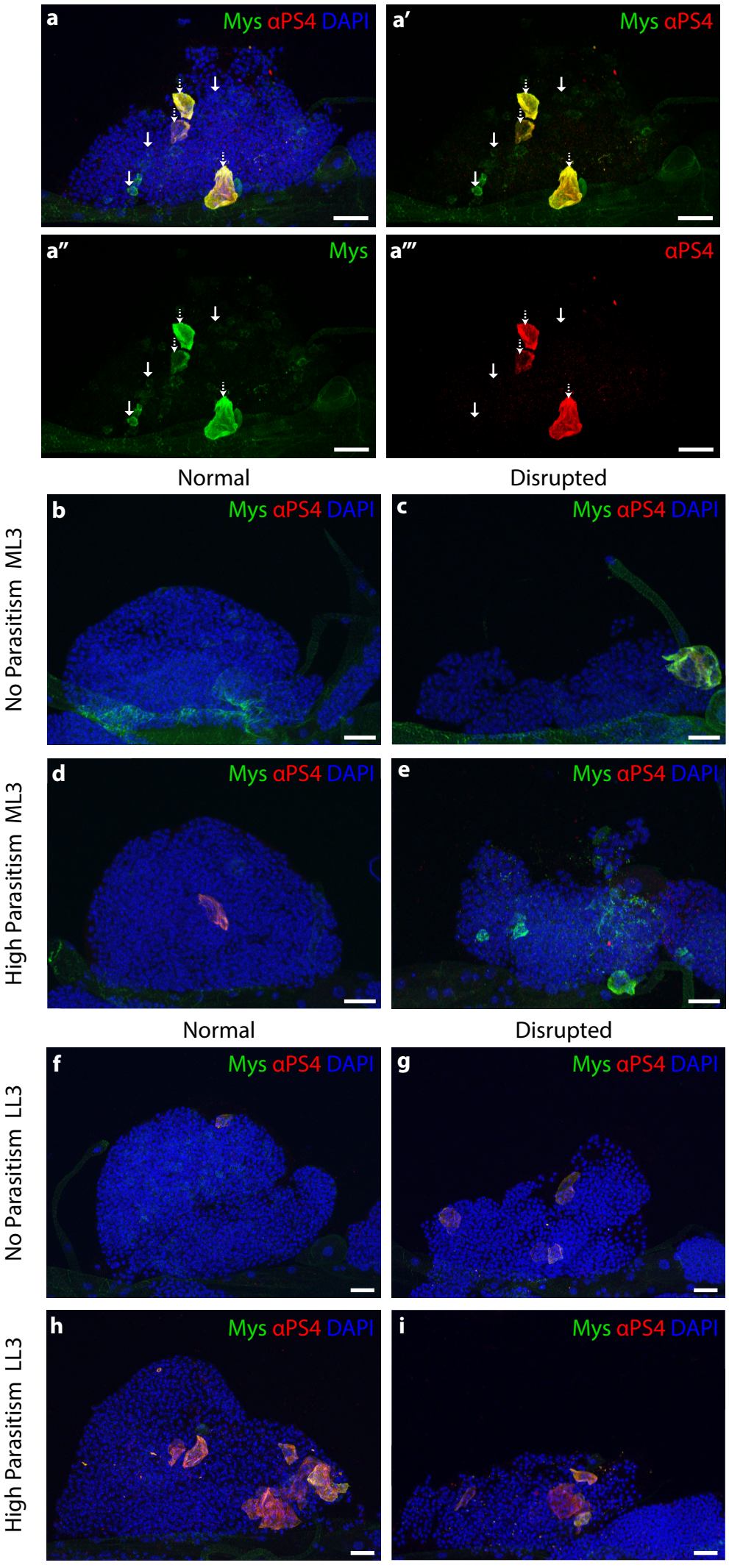
a
Mys αPS4 DAPI
a'
Mys αPS4
a''
Mys
a'''
αPS4
Normal
Disrupted
No Parasitism ML3
b
Mys αPS4 DAPI
c
Mys αPS4 DAPI
High Parasitism ML3
d
Mys αPS4 DAPI
e
Mys αPS4 DAPI
Normal
Disrupted
No Parasitism LL3
f
Mys αPS4 DAPI
g
Mys αPS4 DAPI
High Parasitism LL3
h
Mys αPS4 DAPI
i
Mys αPS4 DAPI

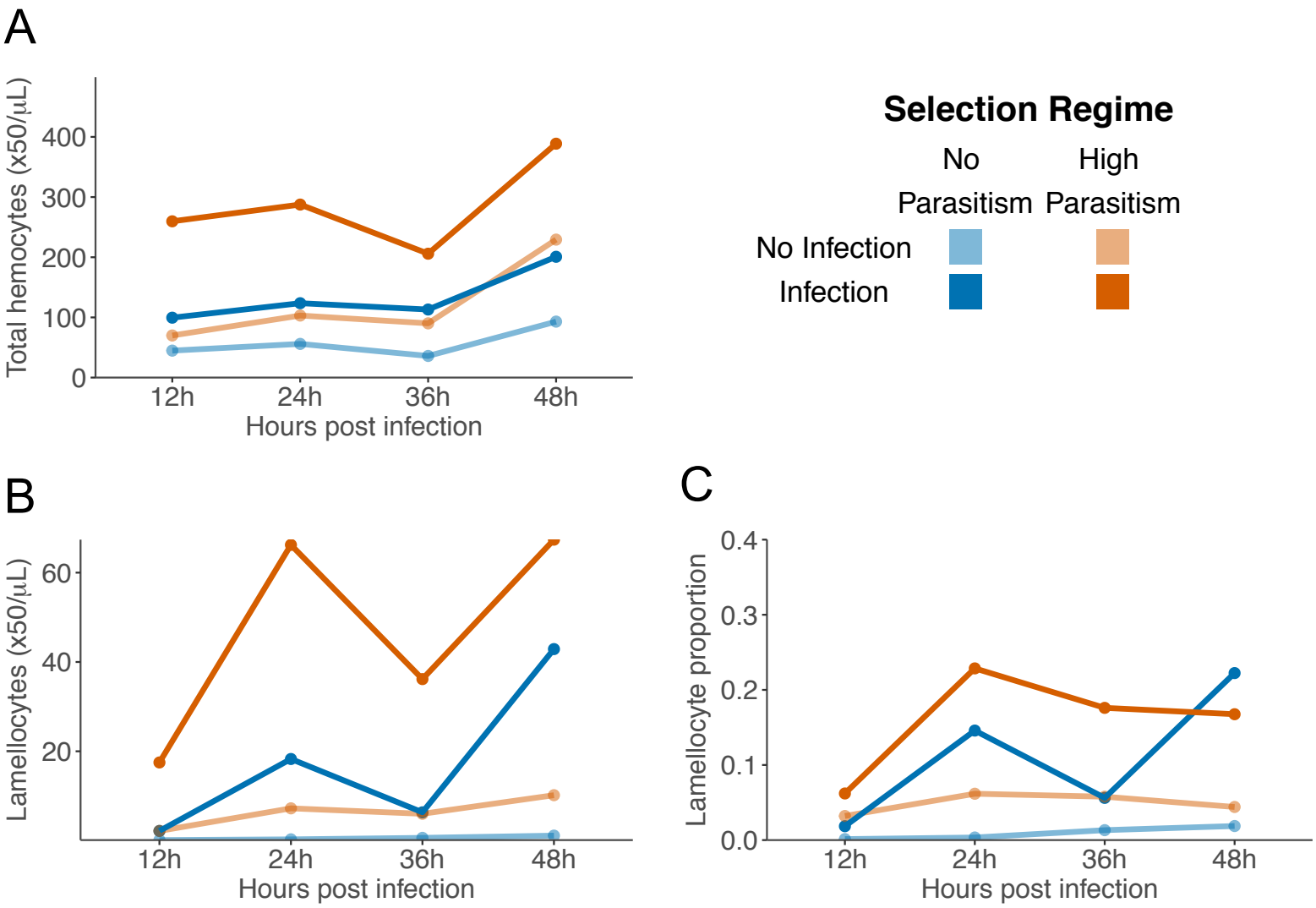
A
Total hemocytes (x50/µL)
400
300
200
100
0
12h
24h
36h
48h
Hours post infection
Selection Regime
No Parasitism
High Parasitism
No Infection
Infection
B
Lamellocytes (x50/µL)
60
40
20
12h
24h
36h
48h
Hours post infection
C
Lamellocyte proportion
0.4
0.3
0.2
0.1
0.0
12h
24h
36h
48h
Hours post infection

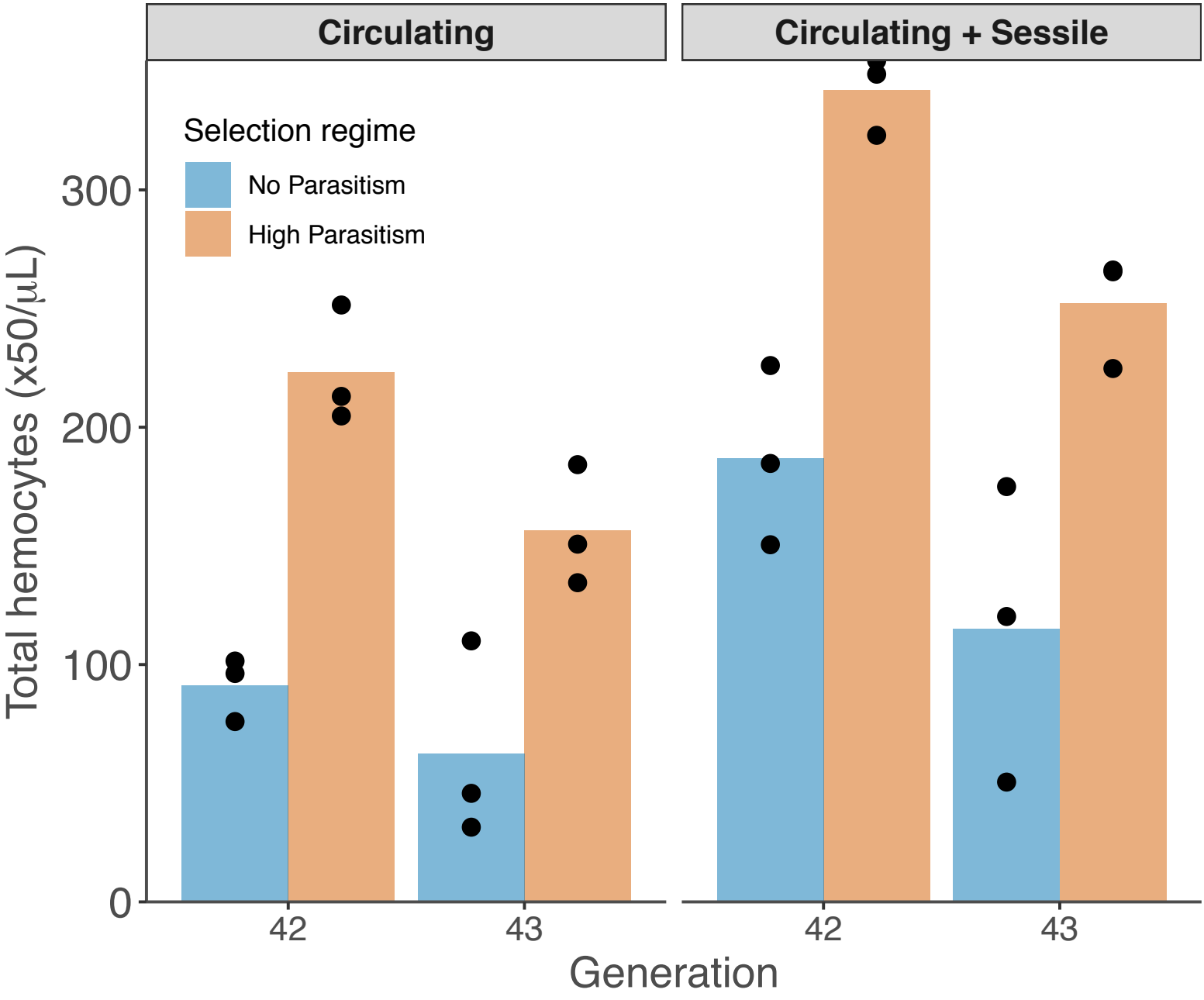
Circulating
Circulating + Sessile
Selection regime
No Parasitism
High Parasitism
Total hemocytes (x50/µL)
300
200
100
0
42
43
42
43
Generation

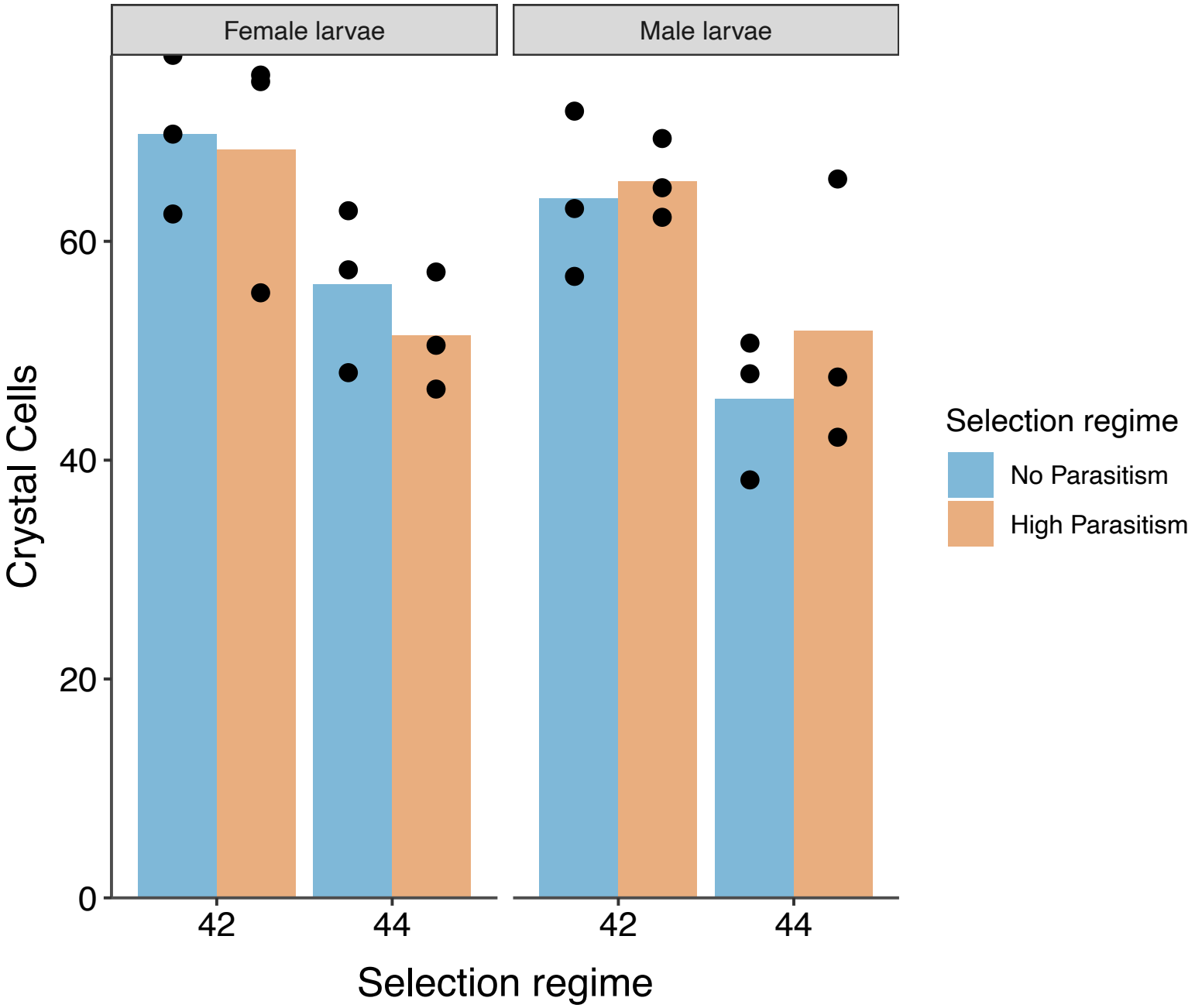
Female larvae
Male larvae
Crystal Cells
0
20
40
60
42
44
42
44
Selection regime
Selection regime
No Parasitism
High Parasitism